Resilience assessment framework for critical infrastructure in a multi-hazard environment: case study on transport assets

Sotirios A. Argyroudis

Dept. of Civil and Environmental Engineering, University of Surrey, UK

& Dept. of Civil Engineering, Aristotle University, Thessaloniki, Greece

Stergios A. Mitoulis

Dept. of Civil and Environmental Engineering, University of Surrey, UK

Lorenzo Hofer, Mariano Angelo Zanini

Dept. of Civil, Environmental and Architectural Engineering, University of Padova, Italy

Enrico Tubaldi

Dept. of Civil and Environmental Engineering, University of Strathclyde, UK

Dan M. Frangopol

Dept. of Civil and Environmental Engineering, Engineering Research Center for Advanced Technology for Large Structural Systems (ATLSS Center), Lehigh University, USA

Abstract:

The exposure of critical infrastructure to natural and human-induced hazards has severe consequences on world economies and societies. Therefore, resilience assessment of infrastructure assets to extreme events and sequences of diverse hazards is of paramount importance for maintaining their functionality. Yet, the resilience assessment commonly assumes single hazards and ignores alternative approaches and decisions in the restoration strategy. It has now been established that infrastructure owners and operators consider different factors in their restoration strategies depending on the available resources and their priorities, the importance of the asset and the level of damage. Currently, no integrated framework that accounts for the nature and sequence

Accepted manuscript: Argyroudis SA, Mitoulis SA, Hofer L, Zanini MA, Tubaldi E, Frangopol DM (2020). Resilience assessment framework for critical infrastructure in a multi-hazard environment. Science of the Total Environment, 714, 136854. https://doi.org/10.1016/j.scitotenv.2020.136854

of multiple hazards and their impacts, the different strategies of restoration, and hence the quantification of resilience in that respect exists and this is an acknowledged gap that needs urgently filling. This paper provides, for the first time in the literature, a classification of multiple hazard sequences considering their nature and impacts. Subsequently, a novel framework for the quantitative resilience assessment of critical infrastructure, subjected to multiple hazards is proposed, considering the vulnerability of the assets to hazard actions, and the rapidity of the damage recovery, including the temporal variability of the hazards. The study puts forward a well-informed asset resilience index, which accounts for the full, partial or no restoration of asset damage between the subsequent hazard occurrences. The proposed framework is then applied on a typical highway bridge, which is exposed to realistic multiple hazard scenarios, considering pragmatic restoration strategies. The case study concludes that there is a significant effect of the occurrence time of the second hazard on the resilience index and a considerable error when using simple superimposition of resilience indices from different hazards, even when they are independent in terms of occurrence. This potentially concerns all critical infrastructure assets and, hence, this paper provides useful insights for the resilience-based design and management of infrastructure throughout their lifetime, leading to cost savings and improved services. The paper concludes with a demonstration of the importance of the framework and how this can be utilised to estimate the resilience of networks to provide a quantification of the resilience at a regional and country scale.

Keywords: resilience, critical infrastructure, environment, multi-hazard, fragility, vulnerability, restoration

1. Introduction

The *exposure* of critical infrastructure to natural hazards such as floods, earthquakes, tsunami, landslides, hurricanes, wildfires or extreme temperatures was proven to have severe consequences on world economies and societies (Pescaroli and Alexander, 2016). For example, the heavy 2007 rainfall in the UK affected the road network, with the cost estimated at £60m, while during the 2009 floods in Cumbria, UK, at least 20 bridges had collapsed or damaged, causing one fatality, £34m of restoration costs and great societal impact (Cumbria County Council, 2010). Among the critical threats to infrastructure around the world, scour is recognised as the most common cause of bridge failure (Kirby et al., 2015). The direct and indirect economic losses due to landslides affecting road networks are of similar magnitude (Winter et al., 2016). The effects of natural hazards may be

exacerbated due to climate change that causes more frequent and intense extreme weather and climatic events (Stern et al., 2013; Draper et al., 2015; Pant et al., 2018; Sarkodie and Strezov, 2019). Furthermore, infrastructure assets are exposed to multiple hazards and/or cascading effects, such as flood series over time, flood-earthquake, earthquake-induced tsunami, landslides and liquefaction, rainfall-induced landslides or earthquake-aftershock events (Akiyama et al., 2019). A well-known example of the importance of multiple hazard effects is the 2011 Tohoku, Japan earthquake and resulting tsunami. During this extreme event, the country rail and highway networks were both strongly affected, and in total 23 stations were washed away, tracks and bridge piers were either eroded or buried, passenger and freight trains were derailed (Krausmann and Cruz, 2013). During the destructive hurricanes Katrina in 2005 and Sandy in 2012 in the US, several structures were damaged due to combined wave forces and debris impact (Padgett et al., 2008). Rainfall-induced landslides are one of the most critical geohazards in the world (Zhang et al., 2019) and earthquake-induced landslides are equally detrimental. The 2008 Wenchuan earthquake in China triggered more than 15000 landslides, caused more than 20,000 deaths and the cut-off of many towns, due to the extensive damage to highways (Tang et al., 2011). More recently, a bridge had collapsed due to flood in Italy, an area with high seismicity (Scozzese et al., 2019).

Infrastructure owners and operators are increasingly faced with the challenge of delivering resilient infrastructure and mitigating the effects of multiple hazards and climate change effects. In particular, resilience describes the emergent property or attributes that infrastructure has, which allows them to withstand, respond and/or adapt to a vast range of disruptive events, by maintaining and/or enhancing their functionality (Woods, 2015). The term is used widely over many different fields of research, but quantitative metrics of the resilience of socio-technical systems are not well established and standards and processes are still emerging (Lloyd's Register Foundation, 2015). The concept of resilient cities and infrastructure for disaster management has nowadays received more attention, and the existing approaches are mainly based on qualitative methods and index systems (Rockefeller Foundation, 2014; Rus et al., 2018). Moreover, the *risk approaches for multi-hazard* assessment and management of ecosystems (Furlan et al., 2018; Robinne et al., 2018), communities (Moghadas 2019; Sajjad and Chan 2019) and critical infrastructure (Giannopoulos et al., 2012; Komendantova et al., 2014; Theocaridou and Giannopoulos, 2015; Chen et al., 2019) are generally qualitative, or quantitative (e.g. Decò

and Frangopol, 2011). Life-cycle design and assessment methodologies of infrastructure under multiple hazards are discussed by Yang and Frangopol (2018) and Akiyama et al. (2019). Also, the hazard interactions and cascading effects can be classified differently, while modelling of multiple hazards has not been established or agreed internationally yet (Gill and Malamud, 2014; Zaghi et al., 2016; Liu et al., 2016; Bruneau et al., 2017).

Resilience-based assessment and management are recent philosophies that are gradually being adopted in practical applications of critical infrastructure and are expected to be incorporated in the next generation of provisions and guidelines, e.g. see REDi system by Almufti and Willford (2013). However, the shift to resilience-based management should include specific methods to define and measure resilience, new modelling and simulation techniques for highly complex and interacting systems, development of resilience engineering and approaches for communication with stakeholders (Linkov et al., 2014). In this context, different frameworks and assessment tools have been proposed in the literature to assess resilience under individual or multiple hazards, at (a) asset level, (b) infrastructure network level, and (c) community or national scale (Table 1). The resilience metrics and criteria are commonly dealing with descriptive and qualitative analysis. Recently, Kong and Simonovic (2019) assessed multiple hazard spatiotemporal resilience of interdependent infrastructure systems using network theory and statistical analysis. Quantitative *resilience metrics* usually measure the quality or performance of the asset or system before and after the event, and the recovery rate (Hosseini et al., 2016). Resilience measures can be either static or time-dependent, and in some cases, stochastic approaches are enabled to account for the aleatoric and epistemic uncertainties (Frangopol and Bocchini, 2011; Ouyang et al., 2012; Decò et al., 2013). The majority of the abovementioned frameworks generally encompass the *principles of resilience or the 4R's,* as per Bruneau et al. (2003): 1) *Robustness*, describing the inherent strength or resistance of a system to withstand external demands, e.g. hazard actions, without degradation or loss of functionality; 2) *Redundancy* (Zhu and Frangopol, 2012), reflecting the system properties that allow for alternate options, choices and substitutions under stresses; 3) *Resourcefulness*, expressing the capacity to mobilise needed resources and services under emergency conditions, and 4) *Rapidity*, defining the speed at which disruption can be overcome.

Accepted manuscript: Argyroudis SA, Mitoulis SA, Hofer L, Zanini MA, Tubaldi E, Frangopol DM (2020). Resilience assessment framework for critical infrastructure in a multi-hazard environment. Science of the Total Environment, 714, 136854. https://doi.org/10.1016/j.scitotenv.2020.136854

Table 1. Indicative literature on resilience assessment frameworks and assessment tools under individual or multiple hazards

Level of analysis	Reference
asset	*Bridges*: Bocchini and Frangopol (2012b), Bocchini et al. (2014), Dong and Frangopol (2015). *Tunnels*: Huang and Zhang (2016)
infrastructure network	*Transport systems*: Saydam et al., (2013), Bocchini and Frangopol (2012a), Hughes and Healy (2014), Chan and Schofer (2015), Kiel et al. (2016). *Water systems*: Mensah and Dueñas-Osorio (2015), Wang et al. (2019). *Energy networks*: Cimellaro et al. (2015). *Airports*: Faturechi et al. (2014). *Interconnected networks*: Fotouhi et al. (2017), Kong and Simonovic (2019)
community-country	Bruneau et al. (2003), Cimellaro et al. (2016), Matthews et al. (2014), Ayyub (2014), Franchin (2018), Zhang et al. (2019)
resilience metrics and criteria	Gay and Sinha (2013), Ouyang and Wang (2015), Mebarki et al. (2016), Hosseini et al. (2016)

The robustness to hazard actions is usually quantified through *fragility functions,* which give the probability of the asset exceeding defined limit states, e.g. serviceability and ultimate, for a given hazard intensity, e.g. peak ground acceleration for earthquakes, water discharge or scour depth for floods or ground displacement for liquefaction and landslides. Fragility functions can be derived from empirical, analytical, expert elicitation and hybrid approaches (Argyroudis et al., 2019; Silva et al., 2019). An overview of the available fragility functions for critical infrastructure subjected to earthquakes is given by Pitilakis et al. (2014), while HAZUS-MH (2011) methodology provides fragility functions and loss models for buildings and infrastructure in the US, exposed to earthquakes, tsunamis, hurricanes and floods. Bridges are key assets of the transport infrastructure, and the available fragility models for earthquakes and other hazards are discussed by Tsionis and Fardis (2014), Billah and Alam (2015), Gidaris et al. (2017) and Stefanidou and Kappos (2019), while fragility functions for other transport assets are summarised by Argyroudis and Kaynia (2014) and Argyroudis et al. (2019). The fragility of other assets exposed to hazards other than earthquakes are limited and sparse, including for example electric power transmission lines and towers exposed to wind (Panteli et al., 2017), industrial plants and tanks subjected to tsunami (Mebarki et al., 2016) or critical infrastructure under volcanic hazards (Wilson et al., 2017). Few fragility models for multiple hazards are available as summarised in Section 2. Hence, despite the increase of research efforts on the vulnerability of critical infrastructure against natural, environmental and human-induced hazards, there is still a lack of systematic vulnerability assessment against multiple hazards, considering also the effects of deterioration, e.g. ageing, and mitigation measures, e.g. retrofitting, in the fragility response.

The rapidity of the recovery after disruption due to a hazard event is expressed through *restoration functions* for the infrastructure assets. The available restoration models correlate the recovery time with the functionality reached for a given damage level, e.g. Gidaris et al. (2017) for bridges, Galbusera et al. (2018) for port facilities, Castillo et al. (2014) for electric power systems, Luna et al., (2011) for water distribution systems and HAZUS-MH (2011) for various infrastructure assets. They are typically based on expert judgments, following a linear, e.g. Bocchini and Frangopol (2012b), stepwise formulation, e.g. Padgett and DesRoches (2007) or normal distribution, e.g. HAZUS-MH (2011). The development of reliable restoration models is a challenge because the recovery time depends on the available resources and practices of the owner, the type of hazard and the extent of the damage. Furthermore, the functionality and restoration time of assets with multiple components, for example, bridges, is dependent on the damage of the sub-components, e.g. bearings, piers, deck, abutments, foundation. This includes different restoration tasks and uncertainties and, therefore, a probabilistic approach is more appropriate. For example, Decò et al. (2013) proposed a probabilistic evaluation of seismic resilience of bridges, accounting for the uncertainties in the recovery pattern, i.e. residual functionality, idle time, duration of recovery and target functionality, as a support tool for decision making within the bridge life-cycle. The restoration times for the different tasks and components can vary considerably, while a range of values or a mean value and a standard deviation can describe the expected recovery time (Bradley et al., 2010; Karamlou and Bocchini, 2017). In general, the restoration models are mainly available for earthquake-induced hazards, while little information for other hazards is provided, e.g. by HAZUS-MH (2011) for tsunami.

Important gaps in current resilience assessment frameworks for infrastructure assets is that they consider only single hazards and one occurrence of the hazard. A more reliable assessment of the vulnerability, risk and resilience of critical infrastructure should consider the occurrence of multiple hazard events, potentially of different natures including their temporal variability during the lifetime of the asset as well as the asset deterioration and/or improvement. The development of methods for lifetime resilience assessment (Yang and Frangopol, 2018) is an urgent need of paramount importance for infrastructure owners and operators, to enhance safety, leading to significant cost savings and efficient allocation of resources toward resilient infrastructure.

This study aims at filling this urgent knowledge gap by (1) providing a sound classification of multiple hazards affecting critical infrastructure, (2) reviewing existing approaches and techniques for dealing with the effect of

multiple hazards in the infrastructure resilience assessment, and (3) developing and applying a resilience assessment framework for critical infrastructure assets exposed to a sequence of individual and/or multiple natural, environmental and human-induced hazard events. This framework considers the factors that reflect redundancy and resourcefulness in infrastructure, i.e. (i) the robustness to hazard actions, based on realistic fragility functions, and (ii) the rapidity of the recovery after the occurrence of different levels of direct damage and induced consequences, based on realistic restoration and reinstatement functions respectively, enabling adjustments to the time of initiation of restoration after the hazard event (idle time), the type of the restoration actions and the sequence of hazards. In Section 2 below, a classification of multiple hazards is given, by also including relevant examples from real systems subjected to hazard sequences. Subsequently, the proposed conceptual framework for resilience assessment is described. The output of the framework is a resilience index, which is a function of the time-variant functionality of the infrastructure over the restoration time for the hazard scenarios. In Section 3, an application of the proposed framework is given by analysing the resilience of a typical highway bridge under two realistic multi-hazard scenarios, both involving the occurrence of a flood and an earthquake event. In the first scenario, it is assumed that the bridge is fully restored after the occurrence of the flood event and before the earthquake strikes the bridge. For the second scenario, the earthquake is assumed to occur during the restoration process following the occurrence of the flood. The results of the resilience assessments for the two cases are presented and discussed in Section 4. The proposed framework and application contribute to the enhancement of current practices for resilience-based management of infrastructure assets by shifting toward the multi-hazard lifetime resilience assessment. The paper concludes with a demonstration of the importance of the framework and how this can be utilised to estimate the resilience of networks to provide a quantification of the resilience at a regional and country scale.

2. Resilience assessment framework for infrastructure exposed to multi-hazard

This section describes the proposed resilience framework for infrastructure assets exposed to multiple hazards. It is recognised that due to the diversity of infrastructure assets and the diversity of hazards and combinations, it will only be realistic if a number of critical scenarios are described, yet, an effort was given for the framework to be holistic and representative for a wide range of critical infrastructure. Section 2.1 introduces a classification

of multiple hazards for critical infrastructure and Section 2.2 describes the proposed framework specifically addressing a sequence of hazards in the resilience assessment.

2.1 Classification of multiple hazards for critical infrastructure

Multiple hazards are classified into three categories. Where appropriate, to simplify the discussion the case of two hazards (Haz-1 and Haz-2) is considered, for which different interaction scenarios are analysed. This classification includes terminology from previous studies, i.e. Gill and Malamud (2014); Bruneau et al. (2017), but also includes the nature of the hazards and introduces the temporal variability of hazard occurrences and restoration measures.

(I) Independent hazards of different impacts, including for example floods caused by different weather phenomena, flood preceding an earthquake or the opposite. The time between the occurrences of the two hazards, their sequence and their intensities can vary considerably. Therefore, depending on the loss of functionality, which defines the residual capacity of the infrastructure asset, the restoration can commence immediately after Haz-1, e.g. a flood, and can be completed before the initiation of the second hazard, e.g. earthquake (Figure 1, left), or the functionality loss due to Haz-1 is not recovered, e.g. the owner does not act or not aware of the loss, until the occurrence of Haz-2, after which the restoration commences (Figure 1, right). Due to the different nature of the hazards, restoration of the damage due to Haz-1, e.g. hydraulic actions, is not necessarily expected to improve the performance against the second hazard, e.g. earthquake. This is a key factor for the resilience-based management for independent hazards and will influence decisions both in retrofitting and restoration schemes, either before or after the hazard incident. Figure 1 (left) represents the expected and desirable strategy of the owner. However, Figure 1 (right), are also said to be realistic scenarios, on the basis of limited resources and, hence, reduced or no reactivity and/or proactivity.

Ecosystems are exposed to more than one hazard, and hence, it is likely that critical infrastructure located in such areas will experience multiple hazards in their lifetime. There are several examples of non-concurrent and independent multiple hazards that caused extensive damage to infrastructure, e.g. in China, the USA, Japan and Europe (Ayyub, 2014; Chang, 2016). Moreover, there are several studies investigating the effect of independent hazards in case of bridges, as for example scour followed by earthquake (Banerjee and Prasad, 2013; Dong et

al., 2013; Wang et al., 2014; Yilmaz et al., 2016; Guo et al., 2016), barge collision and scour (Kameshwar and Padgett, 2018), or earthquake and hurricanes (Kameshwar and Padgett, 2014). Few studies are also available for the risk and resilience assessment of distributed infrastructure exposed to multiple independent hazards, such as for electric power networks under seismic and hurricane hazards by Salman and Li (2018) and road networks under floods, earthquakes and human-induced disasters by Faturechi and Miller-Hooks (2014).

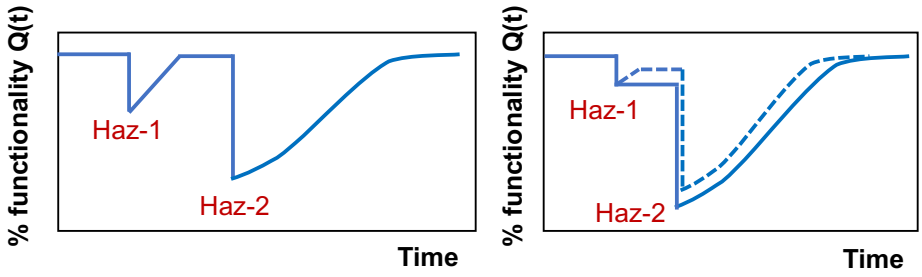

Figure 1. Restoration strategies for a sequence of independent hazards with damage restoration after the occurrence of the first hazard (left) or with partial (dashed line) or no (continuous line) damage restoration after Haz-1 (right).

(II) Correlated or cascading hazards, where the secondary hazard (Haz-2) is triggered by the primary hazard (Haz-1), including, for example, liquefaction, landslide, tsunami and fire triggered by earthquakes, or flood, landslides, extreme wind and debris flow triggered by a hurricane. In this case, the two hazards are concurrent (Figure 2, right) or successive within a short period of time (Figure 2, left). Therefore, the functionality drops due to Haz-1 (solid vertical line in Figure 2) and drops further due to Haz-2 (dashed line in Figure 2) without any restoration taking place after the occurrence of Haz-1. For example, restoration strategies for a bridge constructed in an earthquake-prone area should predict the occurrence of the cascading landslide in a mountainous environment or liquefaction in loose saturated granular soils, both triggered by the ground motion. Another example is the loss of functionality of a bridge due to strong winds during a hurricane, followed by an extensive flood in a short period of time.

Such types of cascading hazards have been extensively observed in past events, including the widespread damage to transport infrastructure due to liquefaction and landslides after the 2007 Niigata – ken Chuetsu Oki earthquake in Japan (Kayen et al., 2009) or the 2008 Wenchuan earthquake in China (Tang et al., 2011). The effects of cascading hazards to infrastructure performance have been studied by Brandenberg et al. (2011) and Aygün et al. (2011) for bridges exposed to liquefaction caused by earthquake shaking, and by Omidvar and Kivi

(2016) for gas pipelines under earthquake, liquefaction and fire following the earthquake. Hackl et al. (2018) and Lam et al., (2018) estimated the impact of rainfall-induced floods and mudflows on a road network considering the associated risks to bridges and pavements, including physical damage and functional loss.

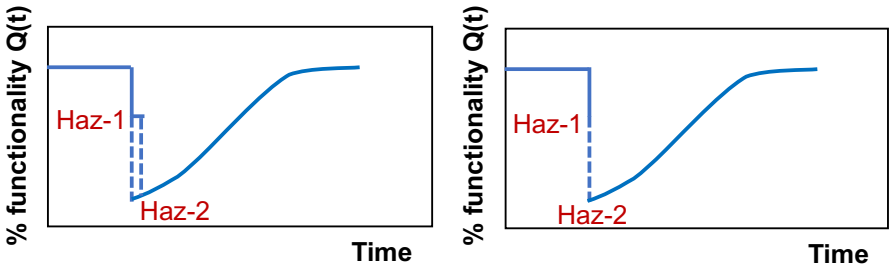

Figure 2. Cascading hazards, where the second (Haz-2) is triggered by the first hazard (Haz-1) simultaneously (right) or within a short period (left) and the restoration commences after the completion of the multiple hazard sequence.

(III) Correlated or independent hazards of the same nature that may have cumulative effects on the structure. Some examples in this category are, e.g. main-shock and aftershocks, or multiple mainshock events occurring during the lifetime of a structure or multiple floods, resulting in scour accumulation at bridge foundations (Tubaldi et al., 2017). For example, scour holes of minor or moderate extent might be forming at bridge foundations throughout the life of the bridge, (Haz-1.1 and Haz-1.2) and then followed by an extensive flood (Haz-1.3) that causes extensive scouring, debris accumulation and hydraulic forces on the structure. The restoration strategy might consider retrofitting before (dashed line) or after (solid line) the major event as shown in Figure 3 (left). The second case described by Figure 3 (right) is the scenario where the major effect occurs first, and then aftershocks take place in a short or longer period after the mainshock, leading to additional loss of functionality. The restoration commencement is strongly dependent on a number of factors including the extent of damage and importance of the asset and potentially influenced by the unpredictable recurrence time.

As an example, after the 2008 Wenchuan earthquake in China, more than 100 major aftershocks were recorded within 72 hours and more than 40,000 aftershocks of variable magnitudes occurred within 6 months after the mainshock (Zhang et al., 2013). Among others, the effects of mainshock-aftershocks in the response and fragility of infrastructure have been studied by Dong and Frangopol (2015) and Ghosh et al. (2015) for bridges, Zhang et al. (2013) in case of gravity dams, and Li et al., (2014) for steel structures. Iervolino et al. (2015) formulated a stochastic process to describe the occurrences of aftershocks and their effect on cumulative

structural damage. To this end, Suzuki et al. (2017) developed state-dependent fragility curves for steel frames based on numerical modelling, calibrated with shake table tests. The fragility of the damaged structure due to mainshock was assessed through a back-to-back IDA using a sequence of ground motions. Kumar and Gardoni (2011) considered cumulative seismic damage in the fragility of RC bridge columns based on a probabilistic model that computes the degraded deformation capacity of the columns as a function of cumulative low-cycle fatigue damage incurred in past earthquakes. More recently, Balomenos and Padgett (2017) analysed the fragility of wharfs subjected to hurricane-induced storm surge and wave loading.

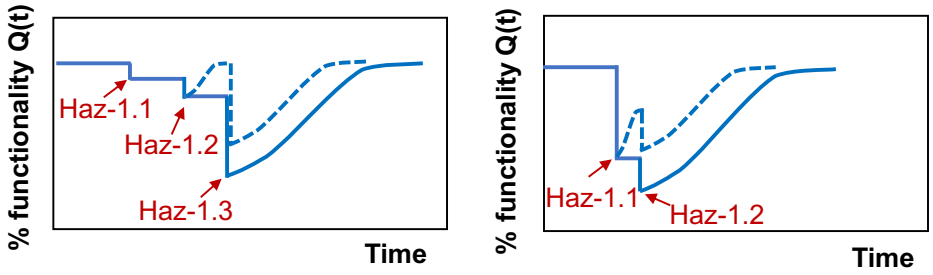

Figure 3. Realistic restoration strategies for correlated or independent hazards of the same nature including sequence of minor damage(s) before the major hazard effect (left) and sequence of a major hazard followed by aftershock(s) of lower intensity (right).

2.2 Resilience framework

A resilience framework is proposed for evaluating losses and resilience of critical infrastructure assets under multiple hazard scenarios including common cases, which are reflecting in the proposed classification of Section 2.1, i.e. (1) the asset is fully restored after the occurrence of Haz-1 and hence when Haz-2 strikes the asset is at each full capacity, (2) the loss of functionality due to Haz-1 is partially restored or (3) remains until Haz-2 occurs. This framework encapsulates redundancy and resourcefulness, i.e. (i) the asset robustness to hazard actions for well-defined critical infrastructure, based on realistic fragility curves or surfaces, and (ii) the rapidity of the recovery after the occurrence of the minor, moderate, major or complete damage, based on realistic reinstatement and restoration functions for the infrastructure assets. The above framework is made adaptive to facilitate timely and cost-efficient management for allocating the resources reasonably and enabling adjustments to the initiation and the type of restoration, the later depending on the hazard(s). This is reflected in the reinstatement and restoration functions, according to the stakeholder requirements and the loss of functionality

after an individual or multiple hazard events. This adaptive approach accounts for the fact that mitigation measures are not always efficient across different hazards as it is further explained below. Furthermore, this approach takes into account the sequence of hazards, and its corresponding impact on the restoration models, taking into account explicitly the time of initiation of the restoration for each hazard considered. The framework consists of four main steps (Figure 4), each described in a subsection and further explained in Figure 5.

i) Multi-hazard analysis

This analysis aims to define the scenario of hazardous events at a site to be considered for resilience assessment. Each hazard can be described through an intensity measure (IM), which quantifies the potential of the event to have an effect on the environment and on the engineering system, and by a series of actions through which it manifests. For example, in the case of floods affecting bridges, the intensity measure could be the water discharge and the actions could include scouring, debris impact, buoyancy, and hydrodynamic forces (Tubaldi et al., 2017). In the case of seismic hazard, the hazard intensity can be described by the peak ground acceleration or the spectral acceleration for the fundamental period of the structural system, which is usually better correlated to structural damage. The action can be described by selecting a set of ground motions scaled to the same intensity level. Usually, hazard curves are developed to describe the probability of exceedance as a function of the intensity measure used to characterize the hazard. The description of the hazard is completed by an occurrence model. The homogeneous Poisson distribution is commonly used to describe the occurrence of natural events in time (Ouyang et al., 2012), though more complex, non-homogeneous models are available, e.g. renewal process for earthquakes (Takahashi et al., 2004; Yeo and Cornell, 2009).

In the case of independent hazard events, e.g. earthquake and floods, hazard curves can be developed separately for each hazard (e.g. Yilmaz et al., 2016). In the case of correlated events, joint distributions need to be assigned to the intensities of the two hazards (e.g. Ming et al., 2015). In the case of cascading events, the probability distribution of the intensity of the second event conditional to the occurrence of the first event of a given intensity should be considered (Marzocchi et al., 2012). In many cases, the hazard rates for the second event are not constant over time and depend heavily on the number of days elapsed since the first event. This is the case for example of mainshock-aftershock sequences, where the aftershock occurrence rates are significantly

influenced by the magnitude of the mainshock and tend to decrease with the increase of time. In the resilience assessment of spatially distributed systems, both the temporal and the spatial relationships of multiple hazards are important (Kong and Simonovic, 2019).

The proposed framework considers a scenario-based approach in the sense that hazard events with a pre-fixed intensity (or return period) are assumed to occur at specific times during the service life of the infrastructure. It is noteworthy that recent frameworks have been proposed that allow a comprehensive, life-cycle assessment of the resilience of infrastructure, by taking into account all the possible events that may affect the system during the design lifetime (Yang and Frangopol, 2018).

ii) Physical vulnerability models

Physical damage is commonly described through fragility functions (see graphs C and D in Figure 5 for individual hazards), which give the probability that the asset exceeds an undesirable limit state for a given intensity of the hazard event to which the asset is subjected, or vulnerability functions, which describe the losses of an asset as a function of environmental/hazard actions as per step i. These functions can be generated based on numerical simulations, empirical data, or expert judgement (see also Section 1.1). The numerical fragility functions are usually built via finite element analyses of the asset under various intensity levels of the hazard. This requires the development of advanced numerical models for critical hazard scenarios, accurately describing the assets' geometrical and mechanical behaviour (Argyroudis et al., 2019). The performance of the components of the asset is measured through Engineering Demand Parameters (EDPs), e.g. drift of bridge columns, settlements under the pavement or embankment, titling of a retaining wall. These EDPs are strongly correlated with damage states (DS) for each asset. In the case of multiple hazards (see graph E in Figure 5), state-dependent fragility models should ideally be made available to describe the asset damage for a given hazard intensity of the second hazard and a given damage level due to the first hazard. These models can be represented as a fragility surface, and quite often the parameter describing the damage due to the first hazard event is replaced by the intensity of the first event (Fereshtehnejad and Shafieezadeh, 2016; Martin et al., 2019). When such models are not available, fragility assessment can be based on engineering judgment by adjusting the fragility

functions of the intact structure. This may entail either reducing the asset capacity or increasing its damage probability due to the preceding damaging event.

Different fragility models are formulated depending on the nature and sequence of hazards. Usually, a two-parameter lognormal function is used to describe the fragility of the component or of a system under a single hazard. The probability of exceeding a particular damage state, DS_i, for a given level $IM=im$ of the hazard intensity (e.g. peak ground acceleration for earthquake or peak flow discharge for flood hazard) can be expressed as per Equation 1:

$$P(DS \geq DS_i | IM = im) = \Phi\left(\frac{ln\left(\frac{im}{\theta_i}\right)}{\beta_i}\right) \quad \text{(Equation 1)}$$

where Φ is the standard normal cumulative distribution function; θ_i denotes the median value of the intensity required to cause the i_{th} damage state, and β_i denotes the logarithmic standard deviation. It is noteworthy that θ_i and β_i generally differ for each damage state. The state-dependent fragility curves are also often assumed to follow a lognormal distribution, with the median value and the lognormal standard deviation depending on both the damage accumulated during the previous event and the intensity of the second hazard event.

In general, vulnerability models for multiple hazards are limited and representative examples from the literature are given in Section 2.1. Adaptive fragility functions account for changes of the asset through its lifecycle, such as (a) *Improvements*, e.g. rip-rap for scour protection or jacketing of columns for seismic retrofitting (e.g. Padgett and DesRoches, 2009). (b) *Deterioration effects*, e.g. ageing effects, such as change of soil material properties due to water content and precipitation history, or corrosion of steel reinforcement (e.g. Argyroudis et al., 2017; Zhong et al., 2012). Changes in hazard intensity and frequency due to *climate change* (Yang and Frangopol, 2019a, 2019b) can be also critical in the fragility and resilience assessment (Dong and Frangopol, 2016). (c) *Cumulation of damage* under repeated events of the same nature (e.g. Ghosh et al., 2015; Iervolino et al., 2016, Tubaldi et al., 2017). In the latter case, the fragility model should account for the reduction in the capacity and functionality of the asset due to the first hazard effect, e.g. the fragility of a damaged bridge after a mainshock earthquake should be shifted to account for the loss in its capacity, thus, aftershocks will strike the affected bridge, not the original one. Hence, Figure 5D reflects a state-dependent fragility surface in this case.

352 The latter statement is also valid for the case where a cascade of hazards emanating from the same cause, but
353 having different impacts occurs, e.g. a tsunami or landslide following a major earthquake. Similarly, the fragility
354 functions of the affected assets should be adjusted to account for Haz-1, because no time is given for
355 intermediate restoration (e.g. Fotopoulou and Pitilakis, 2017 for earthquake-induced landslides). Furthermore,
356 the mitigation or retrofitting measures for restoring damages against a hazard, e.g. flood and scour protection,
357 do not necessarily improve equally the robustness against other hazards of different nature, e.g. earthquake.
358 Ideally, this should be taken into account in the fragility and restoration modelling, as this will affect the
359 resilience of the asset.

360 **iii) Reinstatement and restoration models**

361 The rapidity of the recovery is measured based on reinstatement (for induced consequences) and restoration (for
362 asset damage) models. Reinstatement models provide an estimate of the time required to recover the
363 functionality of an asset after a hazard event, as for example opening and clean-up of a road or railroad,
364 considering natural processes, e.g. surface runoff of rainwater or melting of ice/snow, or intervention actions,
365 e.g. removal of debris or drainage of water (see Figure 5F and 5G for individual hazards). Restoration models
366 correlate the recovery time with the functionality reached for a given damage state (see Section 1.1) and they
367 follow linear, stochastic or stepwise (see Figure 5H and 5I for individual hazards) formulation (e.g. HAZUS-
368 MH, 2011; Bocchini et al., 2012b). Both reinstatement and restoration models are based on previous
369 observations and expert elicitations and should account for the extent of the hazard, the type of asset, the
370 available resources and current practices, and the sequence or cascade of hazards, e.g. flood followed by a debris
371 flow. Depending on the nature of the hazards and their impact on the infrastructure, e.g. loss of functionality,
372 the restoration may have temporal variations changing with the strategy and available resources of the owners
373 or stakeholders as described in Section 2.1. To this respect, probabilistic restoration functions considering the
374 uncertainties in the restoration process can be used (Karamlou et al., 2017; Decò et al., 2013). An important
375 aspect of the restoration models is the idle or lag in the restoration commencement, including emergency
376 response, inspection and condition assessment, site investigation, structural and foundation evaluation, design
377 of measures, and organisational barriers (Mitoulis et al., 2019). The accumulation of damage due to multiple
378 hazard events, i.e. without repairing the damage due to previous events, results to longer reinstatement and

restoration times as shown for example in Figure 5J and 5K, for minor or moderate damage due to Haz-1, followed by minor, moderate or extensive damage due to Haz-2. The restoration time for complete damage due to a combination of hazards is expected to be similar to the time needed to reconstruct an asset when it is completely damaged as a result of the first hazard event, i.e. the restoration curves for one and multiple hazards are the same. The estimation of the recovery time for a combination of induced obstructions (non-structural) and asset damages (structural) is challenging, e.g. rockfalls on a bridge that has been displaced due to scour of the foundation, and this modelling would require parametrisation and adjustment of the proposed framework.

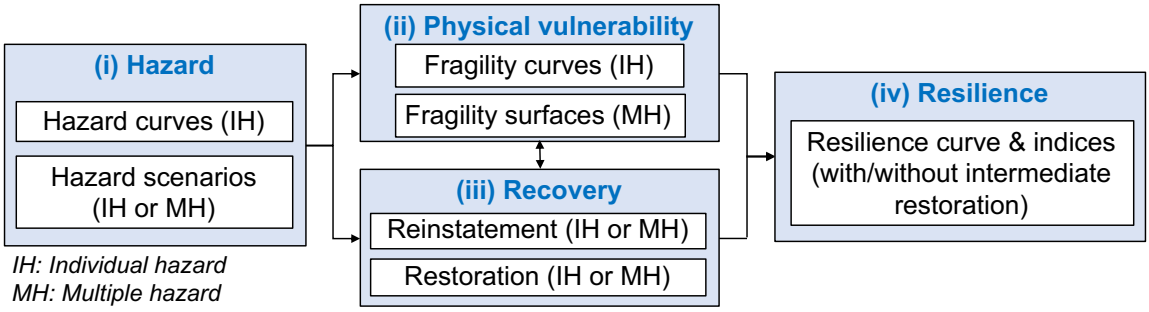

Figure 4. Main steps of the multi-hazard resilience assessment framework (further details given in Figure 5).

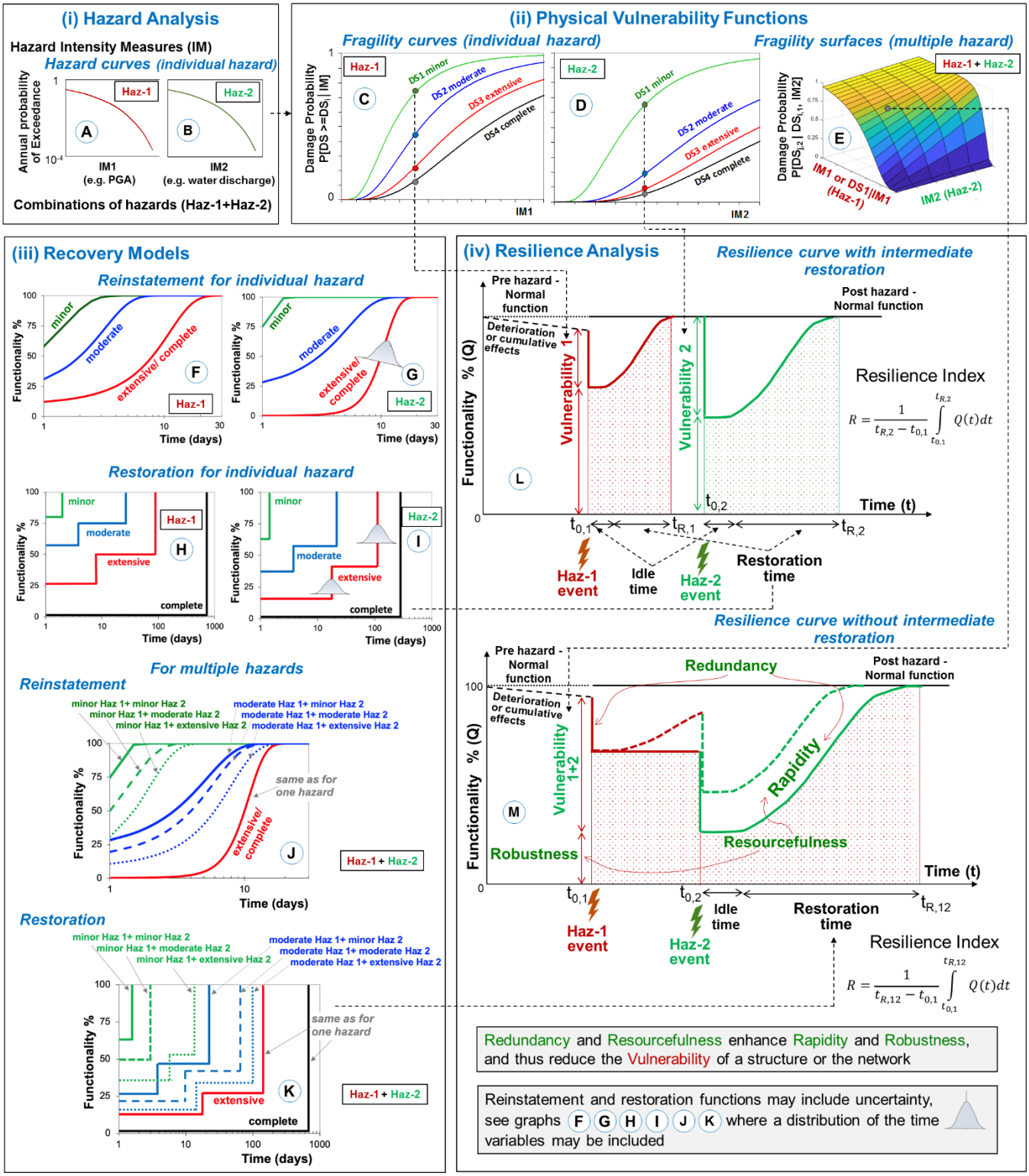

Figure 5. Multi-hazard resilience assessment framework including:

(i) hazard analysis, (ii) physical vulnerability, (iii) recovery, and (iv) resilience analysis.

392

393 **iv) Resilience analysis**

394 This analysis is performed by combining (i) the information on the identified hazards and IMs, (ii) the fragility
395 functions for the asset at hand, and (iii) the restoration models, aiming to generate the resilience curves (Figure
396 5L, 5M) and to assess the corresponding resilience indices. The analysis is adaptable to different sequences of
397 hazards: (1) A series of individual hazard events (Haz-1, Haz-2), where the second hazard occurs after the
398 consequences of the first hazard have been recovered, i.e. $t_{2i}>t_{1f}$, corresponding to Figure 5L, including for
399 example independent hazards of different or same nature within a relatively long period. (2) The second hazard
400 (Haz-2) occurs without (continuous line in Figure 5M) or partial (dashed line in Figure 5M) damage restoration
401 after Haz-1, i.e. $t_{2i}<t_{1f}$, including for example correlated or independent hazards of the same or different nature.

402 To calculate the resilience of the system, it is useful to split the functionality function $Q(t)$ into two parts. The
403 first part of $Q(t)$ for the asset subjected to a hazard event with intensity (IM_1) can be expressed as per Equation
404 2 below:

405 $$Q\left(t\middle|IM_1\right)=\sum_{i=0}^{n_{DS_1}} Q_1\left[t\middle|DS_{i,1}\right]P\left[DS_{i,1}\middle|IM_1\right] \qquad t_{0,1}<t<\min(t_{R,1},t_{0,2}) \qquad \text{(Equation 2)}$$

406 where $Q_1[t|DS_{i,1}]$ is the functionality of the asset subjected to the i^{th} damage state $DS_{i,1}$ due to Haz-1, at time t
407 after the time $t_{0,1}$ of occurrence of the hazardous event, $P[DS_{i,1}\,|\,IM_1]$ is the probability of occurrence of damage
408 state $DS_{i,1}$ as calculated using the fragility functions of step (ii) for the given IM_1 level, n_{DS_1} is the number of
409 possible damage states associated to Haz-1, $t_{R,1}$ is the time when full recovery is achieved after the event, and
410 $t_{0,2}$ is the time of occurrence of the second hazardous event (Haz-2).

411 If the second hazardous event occurs after the system has recovered from Haz-1 ($t_{0,2}>t_{R,1}$), then the second part
412 of $Q(t)$ can be expressed as follows:

413 $$Q\left(t\middle|IM_2\right)=\sum_{i=0}^{n_{DS_2}} Q_2\left[t\middle|DS_{i,2}\right]P\left[DS_{i,2}\middle|IM_2\right] \qquad t_{0,2}<t<t_{R,2} \qquad \text{(Equation 3)}$$

where $Q_2[t|DS_{i,2}]$ is the functionality of the asset subjected to the i^{th} damage state $DS_{i,2}$ of Haz-2, and $P[DS_{i,2} \mid IM_2]$ is the probability of occurrence of damage state $DS_{i,2}$ given the intensity IM_2 of Haz-2.

If Haz-2 occurs during the recovery process after Haz-1 ($t_{0,2} > t_{R,1}$), then the expression of the functionality function becomes more complicated, due to the interaction of the $Q(t)$ due to the two hazardous events, and the second part of $Q(t)$ can be calculated as follows (Equation 4):

$$Q(t \mid IM_2) = \sum_{i=0}^{n_{DS_1}} \sum_{j=0}^{n_{DS_2}} Q_{12}\left[t|DS_{i,1}, DS_{j,2}\right] P\left[DS_{j,2}\middle|DS_{i,1}, IM_2\right] \qquad t_{0,2} < t < t_{R,12} \qquad \text{(Equation 4)}$$

where $Q_{12}\left[t|DS_{i,1}, DS_{i,2}\right]$ is the functionality of the asset at time *t* that needs to recover from damage $DS_{i,1}$ due to Haz-1 and damage state $DS_{i,2}$ due to Haz-2, and $P\left[DS_{j,2}\middle|DS_{i,1}, IM_2\right]$ is the probability of being in damage state $DS_{j,2}$ for Haz-2, conditional to IM_2 and damage state $DS_{i,1}$ with respect to Haz-1, at time $t_{0,2}$, i.e. when Haz-2 strikes the asset. Finally, n_{DS_2} represents the number of the possible damage states associated with Haz-2 and $t_{R,12}$ corresponds to the time of complete recovery from both damages (i.e. $t_{R,12}$ - $t_{0,1}$ is the duration of the recovery). The time between the two hazards can be very short, corresponding to successive or concurrent events, or can refer to longer periods. It is noteworthy that when Haz-2 strikes the asset, some repair works may have already been undertaken. Thus, the level of damage $DS_{i,1}$ at $t = t_{0,2}$ is likely to be less than the damage at $t = t_{0,1}$. The reduction of damage can be assumed to follow the same trend as that of the recovery function, $Q_1(t)$.

In practice, the functionality function Q_{12}, which is required for computing $Q(t \mid IM_2)$ according to Equation 3, is expressed as follows (Equation 5):

$$Q_{12}\left[t|DS_{i,1}, DS_{j,2}\right] = Q_1\left(t|IM_1\right) - \left\{1 - Q_2\left[t - t_{02}|DS_{i,1}, DS_{j,2}, t_{02}\right]\right\} \qquad \text{(Equation 5)}$$

where $Q_1\left(t|IM_1\right)$ denotes the recovery from Haz-1, that continues after the occurrence of Haz-2, and $\left\{1-Q_2\left[t-t_{02}\middle|DS_{i,1},DS_{j,2},t_{02}\right]\right\}$ denotes the functionality losses owed to Haz-2 to the functionality losses, which are also recovered over time.

The resilience assessment is commonly based on a resilience index, which is a function of the time-variant functionality of the infrastructure over the restoration time for the given hazard scenarios (Frangopol and Bocchini, 2011; Ayyub, 2014; Decò et al., 2013). The final expression of the resilience index is given by the following equation:

$$R = \frac{1}{t_h - t_{0,1}} \int_{t_{0,1}}^{t_h} Q(t)dt \qquad \text{(Equation 6)}$$

where t_h is the investigated time horizon. When the time frame of interest is the time to recover from both hazards, then $t_h=t_{R,12}$, which coincides with $t_{R,2}$ if the two hazard events are not interacting one with each other. Since Haz-2 can randomly occur after the occurrence of Haz-1, i.e. at t= $t_{0,2}$, the resilience index computed according to Equation 6, becomes itself a random variable with its moments that need to be evaluated for a complete understanding of the resilience of the asset, i.e. by employing a Monte Carlo approach.

The value of the proposed framework at the asset level is the encapsulation of the loss and recovery process in one index, which can facilitate the efficient allocation of resources, planning and interventions by the owners, toward more resilient infrastructure. Thus, it is essential for the owners to define, with the help of engineers, appropriate thresholds for the resilience indices to expedite the decision-making according to their needs and priorities. The resilience analysis can be extended on a system level (e.g. highway network), accounting for other factors toward a well-informed resilience-based decision making (Zanini et al., 2017; Pregnolato et al., 2018; Arrighi et al., 2019; Akiyama et al., 2019). In this context, the prioritisation of recovery measures should be made on the basis of network analysis, including post-event demand variation during reinstatement/restoration as well as economic, social and environmental consequences due to physical damage and functionality losses, e.g. traffic diversions in transport networks or loss of pressure in water systems.

3. Application to a transport infrastructure asset

3.1 Description of the case study

This section illustrates the application of the framework described above to a realistic case study, consisting of a three-span prestressed concrete bridge, shown in Figure 6, exposed to a sequence of hazard effects (flood and earthquake), which are independent hazards different in nature (category I in Section 2.1). Although the case study does not correspond to any real bridge, it is representative of a very common bridge class. This is a typical fully integral bridge, i.e. has no expansion joints or bearings, with a total length of 101.5m. It has three equal spans of 33.5m, two piers with shallow underwater foundations and two full-height integral abutments. The deck is a box girder and has a total width of 13.5m. The height of the abutments is 8.0m, the footing has a thickness of 1.0m and is 5.5m long. The piers are wall-type sections with dimensions 1.0x4.5m in the longitudinal and transversal direction respectively and a height of 10.0m. The shallow foundation footings have a thickness of 1.5m and 3.5m long. The foundation soil is a very stiff clay, classified as ground type B, according to Eurocode 8-Part 1, while the backfill material is well-compacted sand. For this study, the resilience of the bridge is analysed under the following hazard scenarios: (i) flood only, i.e. scour of the pier on the right, (ii) seismic shaking only, and (iii) flood event followed by earthquake event, considering the temporal variability of the hazard sequences.

3.2 Fragility and functionality loss functions for individual and multiple hazards

The seismic vulnerability of the bridge has been studied by Argyroudis et al. (2018) based on 2D coupled non-linear dynamic analysis of a numerical model that contained the bridge, the two backfills and the foundation soil. The bridge is a high capacity frame structure, and hence, was found to have low vulnerability to seismic shaking. Thus, the collapse of the bridge has a very low probability and may occur only for high levels of seismic intensity. No damage or minor damage is expected on the piers and the prestressed deck, while more significant damage is expected to be of geotechnical nature and is concentrated on the backfill-abutment-wing walls system. Potential failure modes, due to ground shaking, include settlement of the backfill soil, permanent dislocations of the bridge and its foundations and hence, residual stresses within the abutment, the piers and the deck, formation of the bump-at-the-end-of-the-bridge, cracking of the approach slab, excessive soil pressures causing cracking of the abutment, approach slab and wing walls (Elgamal et al., 2008; Murphy et al., 2018).

The finite element model and the procedure employed to develop the numerical fragility curves for the bridge accounting for the effects of flood-induced scour and earthquake loading is described in detail in Argyroudis et al., (2019). Initially, dry conditions were considered for the soil, and then the water table level was gradually raised to 3.0m above the ground surface to simulate flooding conditions. Flooding was accounted for by modifying the properties of the saturated soil layers, while a calibration procedure was followed to account for the dependency of stiffness and damping of the foundation soil on its primary shear strain level during the earthquake. Scour was simulated by removing the soil elements within the scour hole (Tubaldi et al. 2018). Different levels of the scour depth at the foundation of the piers were considered, corresponding to $1.0D_f$, $1.5D_f$ and $2.0D_f$, where D_f =2.5m is the foundation depth. Five real acceleration time histories from earthquakes recorded on rock or very stiff soil were selected as outcrop motion, scaled to different intensity levels for the dynamic analyses. The seismic excitations were induced separately for each scour depth to simulate the combination of the two hazards. The structural damage was defined based on the exceedance of the cracking and yielding moments for critical sections of the deck, pier and abutment. The geotechnical damage was defined based on the maximum permanent ground deformation of the backfill behind the abutment and the foundation of the pier. The fragility of the entire bridge was then extracted assuming a series connection between components (Stefanidou and Kappos, 2017), considering the associated uncertainties.

The parameters of the lognormal fragility functions, i.e. median intensity measure (IM) and lognormal standard deviation, for the different damage states are shown in Table 2, in terms of scour depth (Sc) for flood (FL) and PGA for earthquake (EQ) hazard. The fragility parameters for flood only are largely based on limited numerical analysis without taking into account 3D effects and also contain engineering judgement, to cover the particular needs of this paper.

Table 2. Fragility function parameters (median and lognormal standard deviation) of the case study bridge exposed to flood (FL), earthquake (EQ) and combination (FL+EQ).

Hazard →	**FL**	**EQ**	**FL+EQ ($Sc=1.0D_f$)**	**FL+EQ ($Sc=1.5D_f$)**	**FL+EQ ($Sc=2.0D_f$)**
(1)	(2)	(3)	(4)	(5)	(6)
Damage State	Median Sc [m]	Median PGA [g]			
Minor	2.00	0.32	0.09	0.07	0.01
Moderate	3.50	0.60	0.58	0.16	0.02
Extensive	5.00	1.10	1.05	0.30	0.03
Complete	6.50	1.60	1.56	0.40	0.06

Lognormal standard deviation	0.80	0.70	0.70	0.70	0.70

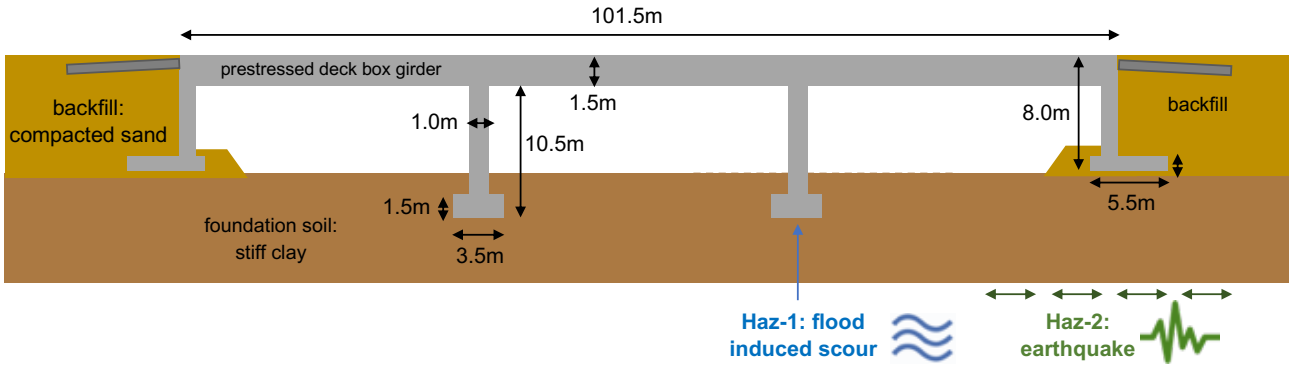

Figure 6. The case study on a highway bridge exposed to flood induced scour (Haz-1) and earthquake excitation (Haz-2).

3.3 Restoration functions for individual and multiple hazards

Reliable restoration models can only be developed based on real asset performances, validated recorded data and evidence and input from experts, e.g. elicitation approaches with participation from owners, stakeholders, and engineers. Secondarily, the availability of materials and resources, labour preparedness, and administration reaction to catastrophes, influence the restoration. For this paper, the repair time for each hazard and damage state has been defined based on engineering judgement considering realistic construction practices and uncertainties. The selection of the restoration time was made on the basis of the bridge typology and geometry, as well as the failure modes considered in the fragility analysis. A detailed presentation of the failure modes and restoration tasks for each damage state is shown in Figures 7 and 8, for flood and earthquake hazards. The common restoration tasks include engineering, administration and structural health monitoring tasks, while the restoration works are differentiated into structural and geotechnical. The relatively short restoration time for complete damage due to seismic shaking only is related to the low vulnerability of the specific bridge type - integral and robust, whilst the expected damage is mainly of geotechnical nature and is concentrated on the backfill-abutment-wing walls system, which is easily restored. The restoration times for the individual and the combined hazards are summarized in Table 3, where a mean and standard deviation are provided assuming that the restoration functions follow a normal distribution. Idle time is also considered, corresponding to the time from the occurrence of the event to the commencement of the restoration works.

Accepted manuscript: Argyroudis SA, Mitoulis SA, Hofer L, Zanini MA, Tubaldi E, Frangopol DM (2020). Resilience assessment framework for critical infrastructure in a multi-hazard environment. Science of the Total Environment, 714, 136854. https://doi.org/10.1016/j.scitotenv.2020.136854

For the combined hazards, the restoration time is defined assuming that the restoration commences after the occurrence of the second hazard, i.e. earthquake, without having taken any restoration measures after the occurrence of minor or moderate damage due to the first hazard, i.e. flood, as per Figure 1 (right). A pragmatic approach for the restoration models should consider that significant damage will be dealt with by the owner, and hence, it was considered to be unrealistic to have a bridge extensively or completely damaged after a flood (Haz-1), without any measures being taken prior to the earthquake (Haz-2). Thus, Figure 1 (left) is more likely to illustrate the case where Haz-1, i.e. flood, causes extensive or complete damage, in which case the asset will be restored partially or fully. In this case, a reasonable approach is to reconstruct the fragility functions of the restored bridge for the second hazard, i.e. earthquake, as the asset is now expected to respond differently from the initial pre-flood undisturbed asset. For this research, it was considered that the fully restored bridge has the same performance as the undisturbed bridge, an assumption that is subject to further research. Also, the resilience curves are based on the assumption that the functionality of the bridge is only affected by the portion of the functionality that has been lost and not by the nature of the hazard. Thus, for example, a 20% loss of functionality due to flood followed by a 10% loss of functionality due to an earthquake, means a total loss of functionality of 30%. Nevertheless, the restoration times are differentiated based on the nature of the hazards.

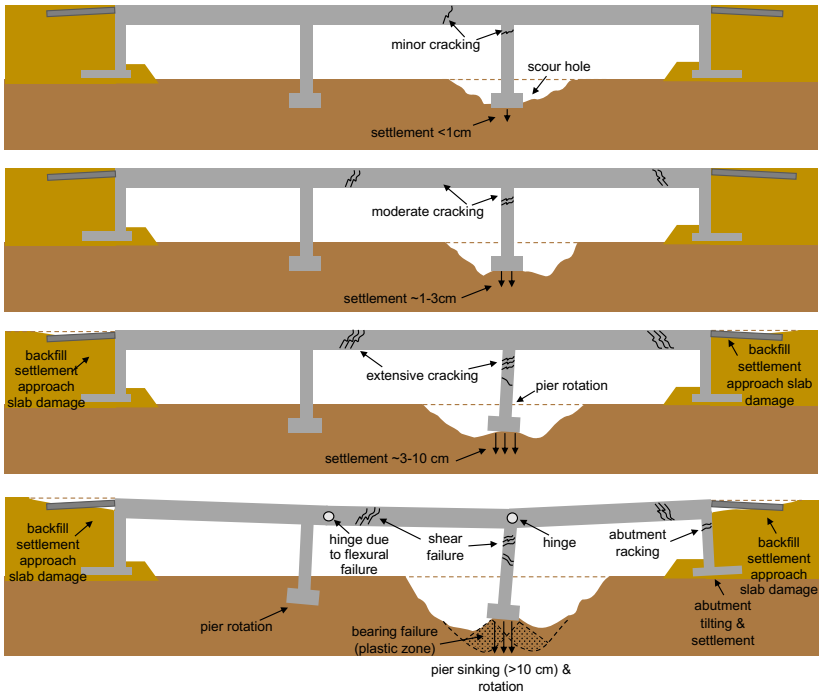

Minor damage

Restoration tasks:
STR: repair cracks and spalling with epoxy and/or concrete
GEO: rip-rap and/or gabions for filling of scour hole and scour protection

Moderate damage

Restoration tasks:
STR: repair cracks and spalling with epoxy and/or concrete
GEO: rip-rap and/or gabions for filling of scour hole and scour protection

Extensive damage

Restoration tasks:
STR: repair cracks and spalling with epoxy and/or concrete; realignment of pier; jacketing
GEO: erosion protection measures; rip-rap and/or gabions for filling of scour hole and scour protection; installation of deep foundation system

Complete damage

Restoration tasks:
STR: demolition of existing, reconstruction of new bridge,
GEO: scour and erosion protection measures

Common tasks for all damage states:
ENG: emergency inspection; site investigation and assessment; preliminary design; detailed design; advisory services during construction;
ADM: contract administration;
SHM: monitoring and inspection during construction; monitoring after the completion of repairs

Type of tasks:
ENG: engineering; ADM: administrative;
STR: structural; GEO: geotechnical;
SHM: structural health monitoring

542

543 **Figure 7**. Damage states and restoration tasks for local scour effects on bridge pier shallow foundation.

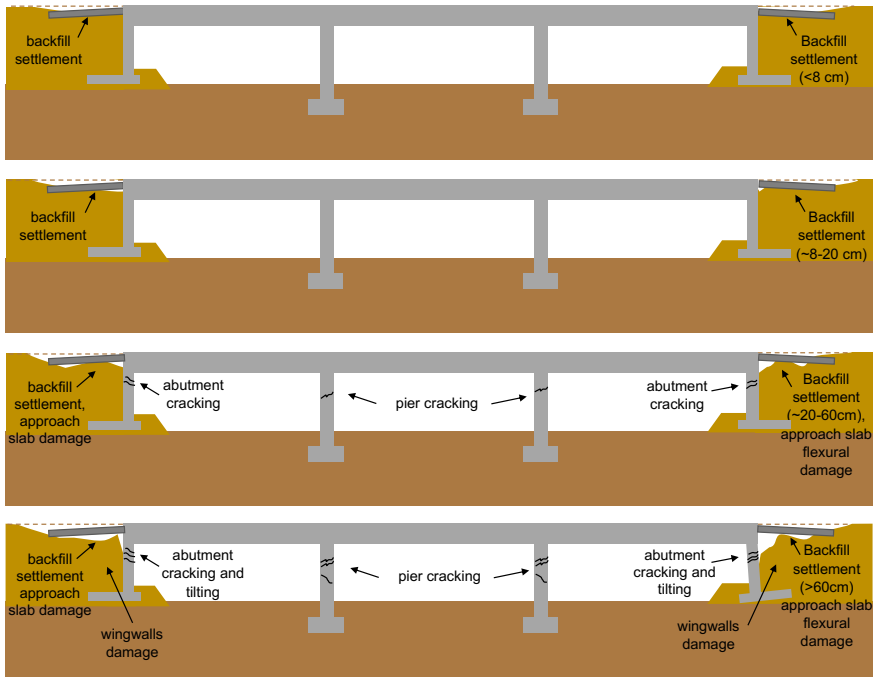

Minor damage

Restoration tasks:
GEO: filling of the backfill gap; repair of road pavement

Moderate damage

Restoration tasks:
GEO: filling of the backfill gap; repair of road pavement and approach slab

Extensive damage

Restoration tasks:
STR: repair of cracks and spalling with epoxy and/or concrete
GEO: filling of the backfill gap, repair of road pavement and approach slab

Complete damage

Restoration tasks:
STR: repair of cracks and spalling with epoxy and/or concrete, realignment of the abutment
GEO: filling of the backfill gap, repair of pavement, approach slab, wingwalls,

Common tasks for all damage states:
ENG: emergency inspection; site investigation and assessment; preliminary design; detailed design; advisory services during construction; ADM: contract administration;

Type of tasks:
ENG: engineering; ADM: administrative;
STR: structural; GEO: geotechnical

544

545 **Figure 8.** Damage states and restoration tasks for seismic effects on a bridge with shallow foundations.

546 **Table 3.** Parameters of the restoration functions (mean time and standard deviation) for the case study bridge exposed to
547 flood (FL), earthquake (EQ) and combined (FL+EQ) hazards.

Hazard:	**FL**			**EQ**		
Damage state	**Mean restoration time [days]**	**Standard deviation [days]**	**Idle time [days]**	**Mean restoration time [days]**	**Standard deviation [days]**	**Idle time [days]**
Minor	7	8.4	3.5	2	2.4	3.5
Moderate	15	13.5	7.5	7	6.3	7.5
Extensive	30	18	15	14	8.4	15
Complete	200	80	100	45	18	1000

548

Hazard:	**FL+EQ**			
Scour	**Damage state (EQ)**	**Mean restoration time [days]**	**Standard deviation [days]**	**Idle time [days]**
Minor Sc = 1.0 D_f	Minor	5	5	1
	Moderate	10	9	3
	Extensive	20	14	12
	Complete	50	16	24
Moderate Sc = 1.5 D_f	Minor	10	10	2
	Moderate	20	18	6
	Extensive	40	28	24
	Complete	80	32	48
Extensive Sc = 2.0 D_f	Minor	30	30	6
	Moderate	60	54	18
	Extensive	100	70	60
	Complete	160	64	96
Complete	Minor / Moderate / Extensive / Complete	200	80	100

549

550 ### 3.4 Modelling and quantification of resilience and results

551 This section contains the results of the analyses performed to the case study previously illustrated, to highlight
552 the impact of consecutive hazards, i.e. flood and earthquake events, on the final bridge resilience index. For this
553 application and all the cases presented herein, it was assumed that flood hazard occurs first (Haz-1) and
554 earthquake second (Haz-2). Moreover, the earthquake event is assumed to happen before (as shown with the
555 dashed line in Figure 1, right) or after (as shown in Figure 1, left) the end of the recovery process following a
556 flood. All cases are investigated by assuming three different scour levels, 1.0 D_f, 1.5 D_f, and 2.0 D_f and five
557 levels of peak ground acceleration (PGA), 0.2g, 0.4g, 0.8g, 1.2g and 1.6g. The bridge resilience curves *Q(t)*

558 have been computed according to equations 2 and 3 provided in Section 2.2, and the resilience index *R* has been
559 calculated based on Equation 6.

560 Figure 9 shows the results of the first case in which seismic scenarios of different magnitude are considered to
561 occur after the complete bridge recovery from Haz-1 ($t_{02} = t_{h1}$). In all cases, namely 1.0 D_f, 1.5 D_f and 2.0 D_f,
562 the time needed for recovering from the flood is significantly higher than the time for the full restoration for
563 any PGA level as reflected in the restoration tasks of Figures 7 and 8 and the restoration time described in Table
564 3. However, the loss of functionality due to Haz-1 is limited when compared to the one caused by the higher
565 PGA levels. In general, the resilience of the bridge decreases with increasing levels of scouring and PGA.

566

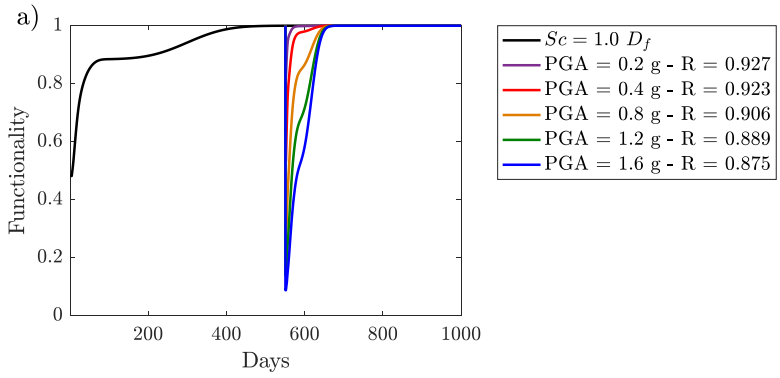

567

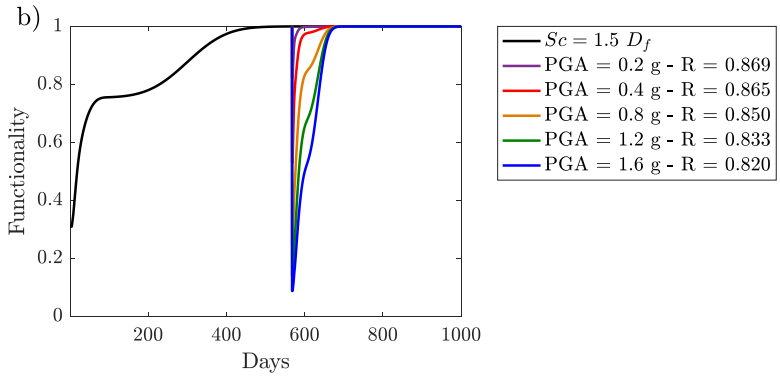

568

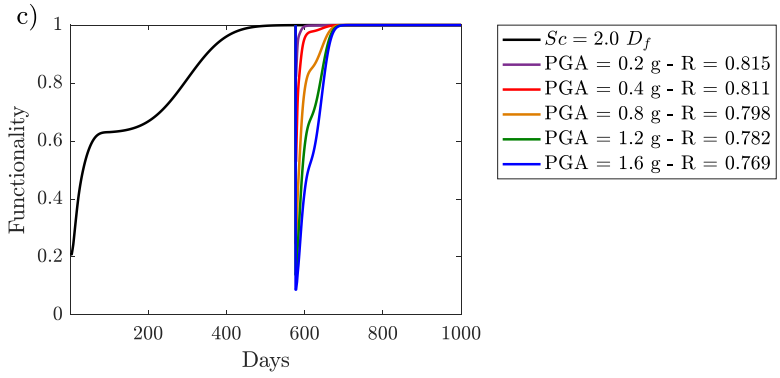

Figure 9. Resilience curves for the case that Haz-2 (EQ at PGA levels equal to 0.2. 0.4, 0.8, 1.2 and 1.6 g) occurs after the total recovery from Haz-1: a) Sc = 1.0 D_f, b) Sc = 1.5 D_f, and c) Sc = 2.0 D_f.

The second case considered corresponds to the occurrence of Haz-2 when the recovery from the previous calamitous event is still ongoing ($t_{0,2} < t_{R,1}$). This second case is more complex than the first since the effect on the total bridge recovery is strongly influenced by the temporal occurrence of the seismic event. Since the time of occurrence of Haz-2 is a random variable (RV), the restoration process and the resilience index R itself becomes random. For computing the distribution of R, the time of occurrence of Haz-2 has been uniformly sampled in the time interval between the occurrence of Haz-1 and the time of total recovery from Haz-1. Figure 10 describes the steps of the numerical simulation framework, which has been developed in Matlab (2017) on the basis of a Monte Carlo approach. In particular, 15,000 recovery curves have been sampled for each combination of D_f and PGA, ensuring precision of the estimator of 0.02. Regarding the parameters for the damage state-dependent fragilities, these have been estimated based on a linear interpolation over time between two extreme values for the following cases: (a) the case of FL+EQ without any intermediate restoration (columns 4, 5, 6 in Table 2), which is the lower bound, and (b) the case of EQ only (column 3 in Table 2), which is the upper bound. A similar approach was adopted for the restoration function parameters, i.e. interpolating the corresponding mean restoration time, between the lower (FL+EQ) and the upper (EQ) bounds.

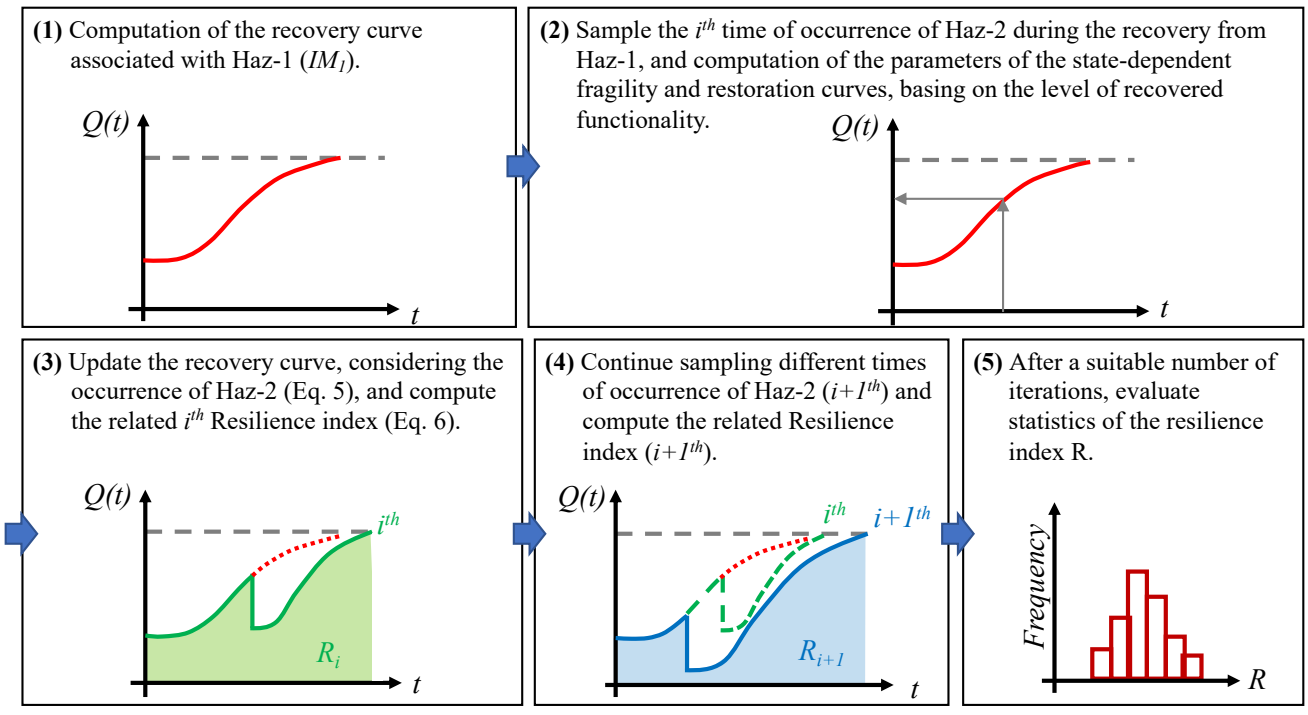

Figure 10. Numerical simulation framework developed in Matlab (2017) including the steps for the resilience assessment, for the case where Haz-2 occurs during the recovery from the previous calamitous event (Haz-1).

Figure 11 shows the effects of five different levels of PGA, randomly occurring during the recovery from Haz-1. In particular, in the case with the lower level of PGA, i.e. 0.2 g, a minor shaking soon after the flood is sufficient for dropping the bridge functionality to zero. This is caused by a combination of a low post-flood initial functionality and high bridge seismic vulnerability due to the short time between the two hazards occurrence. For all five cases, the effect of the earthquake on the resilience lowers when it occurs a long time after the occurrence of the previous Haz-1, and this is clearly shown by the grey curves representing the entire sampled recovery curves. For high PGA levels, greater than 0.8 g, the residual functionality drops to zero even when the earthquake occurs almost at the end of the restoration process. Figure 12 shows the second case in which an earthquake occurs after a flood event able to cause a scour equal to 1.5 D_f. With a scour of 1.5 D_f, a PGA equal to 0.2 g, occurring when 35% of the lost functionality is recovered, can cause a complete loss of the bridge functionality. Higher levels of PGA can significantly compromise the bridge functionality even when occurring for an intermediate level of recovered functionality. Figure 13 shows the case in which a significant flood occurs, causing a scour of 2.0 D_f. In this case, the bridge's structural capacity is severely compromised and also lower values of PGA are sufficient for causing an extensive or complete damage state. This case represents the worst-case scenario, in which there is a significant bridge functionality drop due to Haz-1, together with a significant increase of the seismic vulnerability and of the recovery time also after the earthquake. Even in this case, the time of occurrence of Haz-2 plays an important role; indeed, the worst situation is when there is the rapid succession of the two hazards, while the less impacting is when Haz-2 occurs at the end of the recovery process from Haz-1.

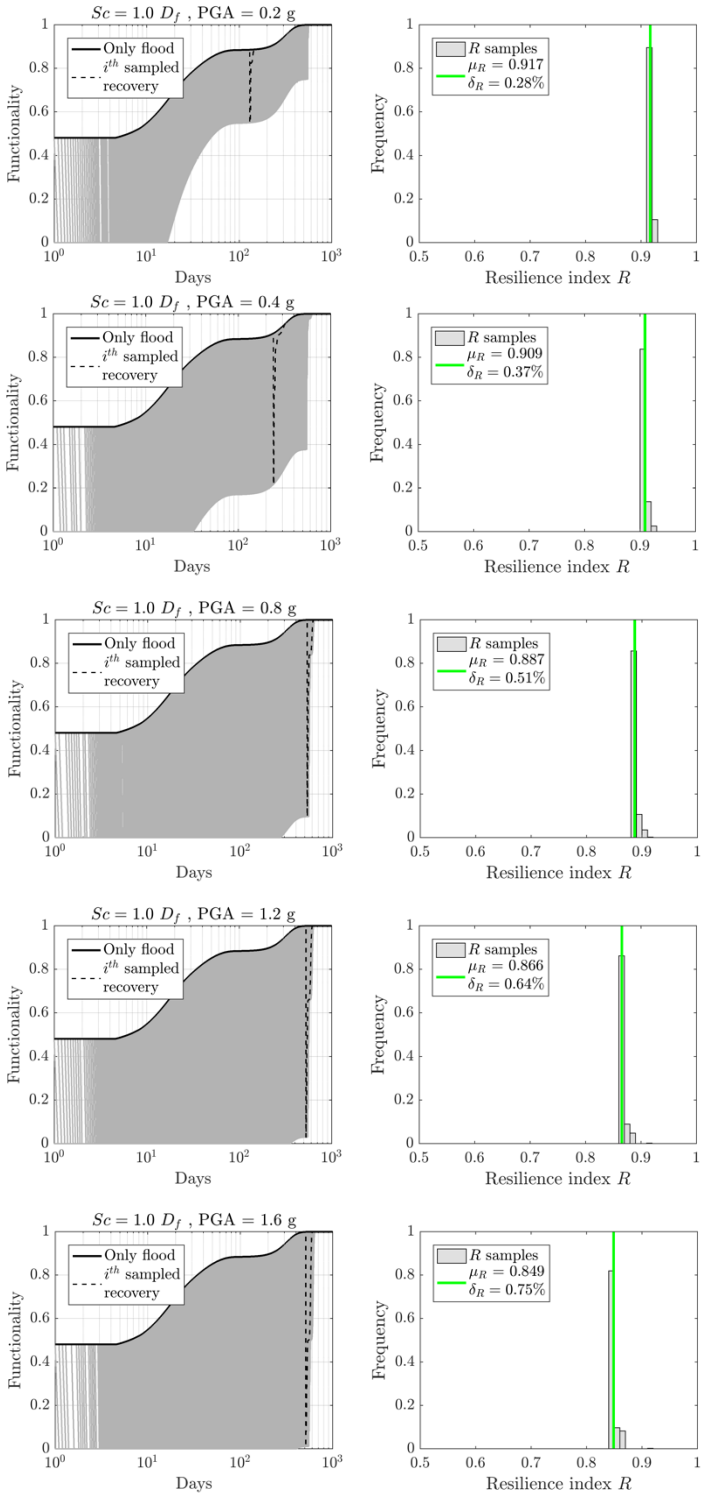

Figure 11. Resilience curves for the case that Haz-2 (EQ at PGA levels 0.2. 0.4, 0.8, 1.2, and 1.6 g) occurs during the recovery phase after Haz-1 (FL), with Sc = $1D_f$. The grey lines in the plots at the left correspond to the 15,000 recovery curves sampled in the time interval between the occurrence of Haz-1 and the total recovery from Haz-1. μ_R and δ_R in the plots (right), correspond to the central value and the coefficient of variation of the estimated resilience indices.

618

619

620

621

622

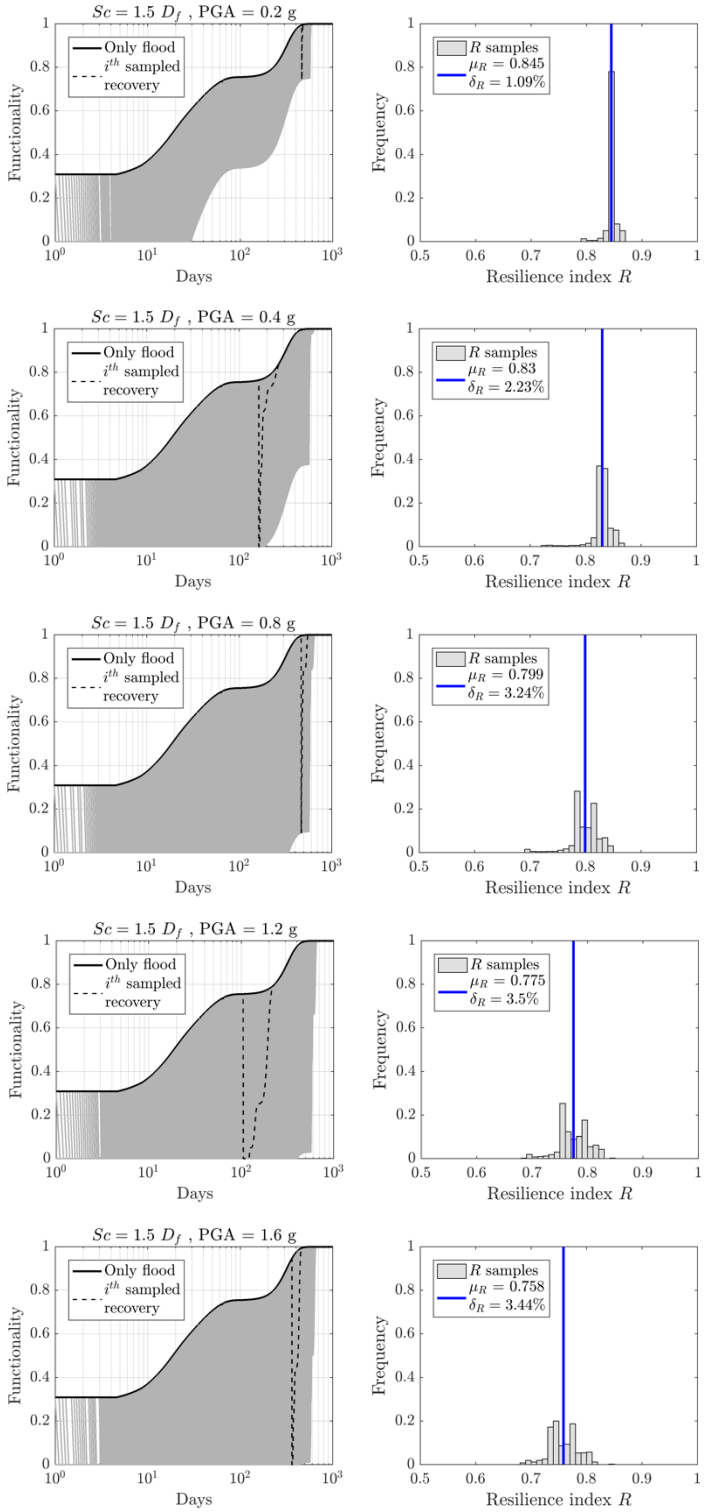

623 **Figure 12.** Resilience curves for the case that Haz-2 (EQ at PGA levels 0.2. 0.4, 0.8, 1.2, and 1.6 g) occurs during the
624 recovery phase after Haz-1 (FL), with Sc = 1.5 D_f. The grey lines in the plots at the left correspond to the 15,000
625 recovery curves sampled in the time interval between the occurrence of Haz-1 and the total recovery from Haz-1. μ_R and
626 δ_R in the plots (right), correspond to the central value and the coefficient of variation of the estimated resilience indices.

627

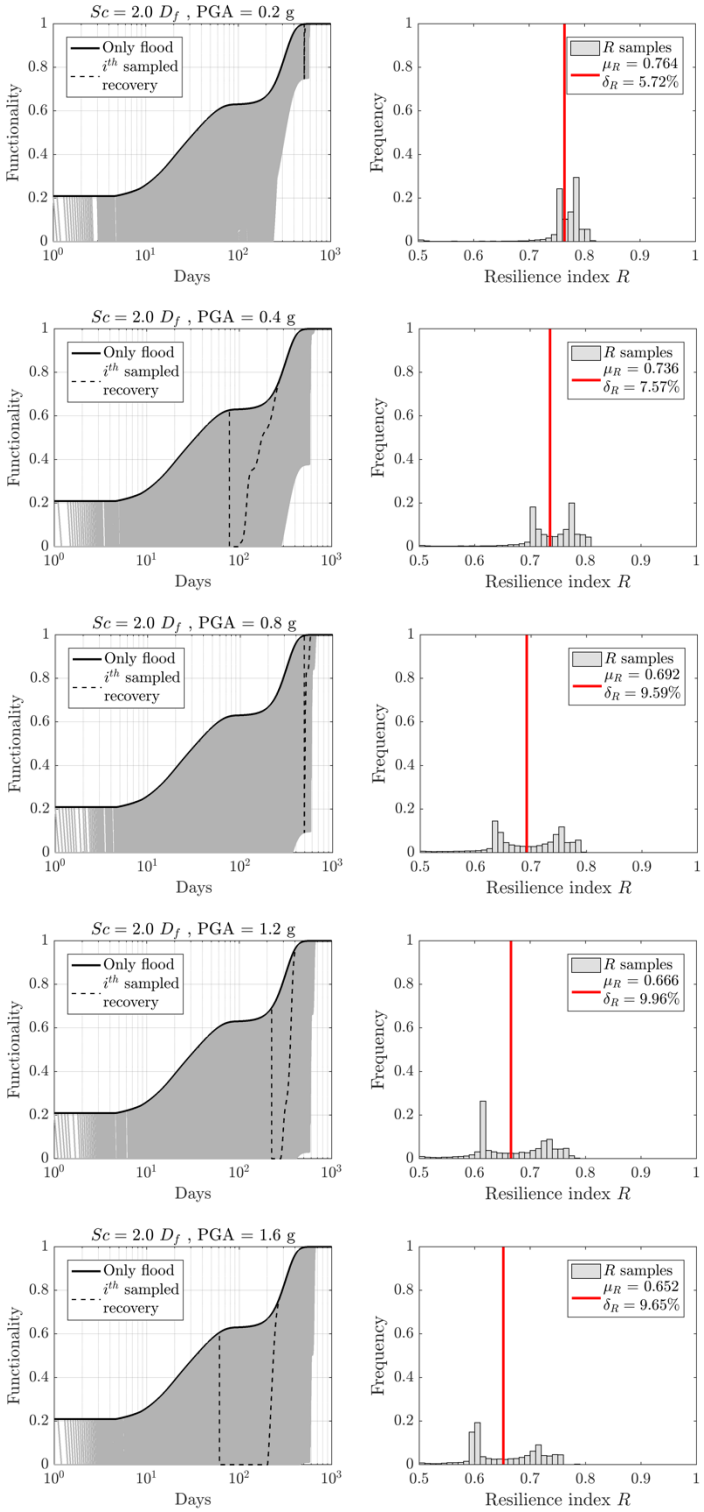

Figure 13. Resilience curves for the case that Haz-2 (EQ at PGA levels 0.2. 0.4, 0.8, 1.2, and 1.6 g) occurs during the recovery phase after Haz-1 (FL), with Sc = 2.0 D_f. The grey lines in the plots at the left correspond to the 15,000 recovery curves sampled in the time interval between the occurrence of Haz-1 and the total recovery from Haz-1. μ_R and δ_R in the plots (right), correspond to the central value and the coefficient of variation of the estimated resilience indices.

Figure 14 illustrates the joint influence of the levels of scour and PGA on the resilience index. In particular, the effect of the earthquake is more relevant when occurs with a higher level of scour. Furthermore, the evaluation of the entire resilience index distribution allows quantifying the uncertainty correlated to the occurrence of Haz-2 with respect to Haz-1. This has been done by introducing the coefficient of variation $\delta = \sigma/\mu$, usually preferred to the common variance (or standard deviation) since the measure of variability is more meaningful if measured relative to the central value μ, and δ is always positive. Besides, the distribution of R allows a reliability-based assessment of bridge resilience. Bounds on the resilience indexes in Figure 13, show that the estimation of R is more uncertain for increasing levels of scour and PGA. For this particular case study, it was found that the resilience index R will obtain a maximum value of 0.77 if the two hazards (FL & EQ) are considered independent, whereas the same index yielded a value of 0.65 ± 0.07 when EQ event occurred during the restoration after FL. The latter corresponds to the severe scenario of maximum scour depth and PGA intensity, while this error is minimised for smaller intensities of the two hazards. The relatively high values of R even for severe earthquake intensities are due to the high robustness of this specific bridge. Results show the need for probabilistic approaches for the resilience assessment, especially for combined extreme events, for which the temporal occurrence can play a key role.

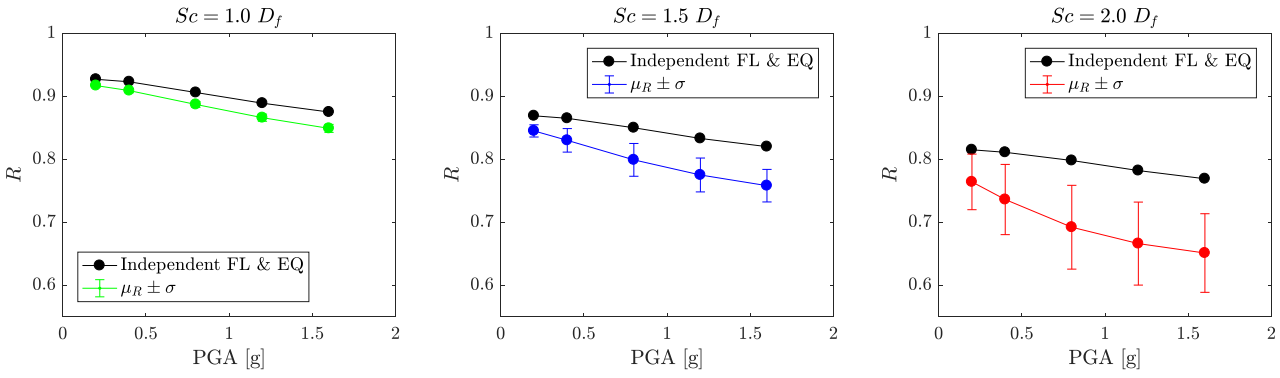

Figure 14. Comparison between resulting resilience indexes for all the investigated scenarios: a) FL (Sc = 1 D_f) +EQ, b) FL (Sc = 1.5 D_f) + EQ, b) FL (Sc = 2.0 D_f) + EQ. In the black curve, EQ (Haz-2) occurs after the complete restoration of FL (Haz-1) induced damages. In the green, blue and red curves, EQ occurs during the restoration of FL induced damages.

Finally, Figure 15 shows the behaviour of the expected value of R, E[R], and the coefficient of variation, $\delta(R)$, as a function of the scour D_f and the shaking level. For this specific case study, the trend of the resilience index

can be well represented by a plane, where the expected R values decrease for increasing Sc and PGA. Regarding δ, the variable that most affects the coefficient of variation is the level of scour.

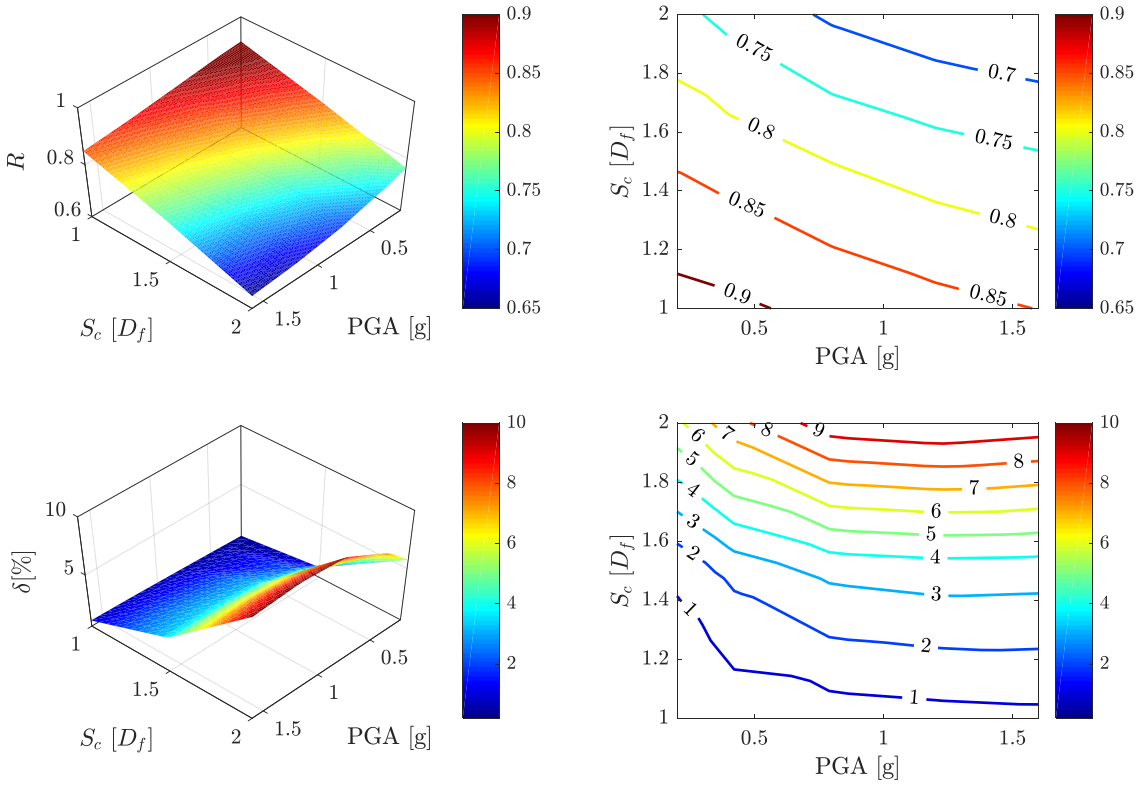

Figure 15. Behaviour of the resilience index, μ_R, (plots at the top) and the coefficient of variation, δ, (plots at the bottom) as a function of the scour (Sc) and the shaking level (PGA).

3.5 Roadmap for resilience assessment of critical infrastructure at the network and national scale

The proposed resilience assessment framework has been applied to a highway infrastructure asset, i.e. a river crossing bridge exposed to flood and earthquake events. However, this approach can be adjusted, extended and applied to the entire highway infrastructure of a region or a country as per Figure 16, i.e. to a portfolio of critical highway assets such as bridges, tunnels, embankments, slopes or retaining walls. Likewise, it can be employed in the resilience evaluation of critical infrastructure, such as hubs, ports, airports, railways, electric power or gas networks toward community resilience (Ayyub, 2014; Cimellaro et al., 2016). This roadmap in achieving resiliency in regions, countries or continents, is aligned with international frameworks and policies for disaster risk reduction, e.g. UNISDR, 2015; NIST, 2016; Rockefeller Foundation, 2019; Lloyd's Register Foundation, 2019. In this respect, the resilience assessments for single or multi-hazard events at infrastructure scale can be

utilised by the network operators and owners to prioritise the mitigation measures, including retrofitting and/or monitoring of critical assets, optimisation of recovery strategies and disaster preparedness, insurance of the infrastructure against losses from natural and/or human-induced disasters, and planning for extending infrastructure. Decision making may be based on the resilience assessment, accounting for critical interdependencies between networks, and other factors, such as socio-political criteria, the impact of infrastructure failures to businesses, populations and environment (Cimellaro et al., 2010).

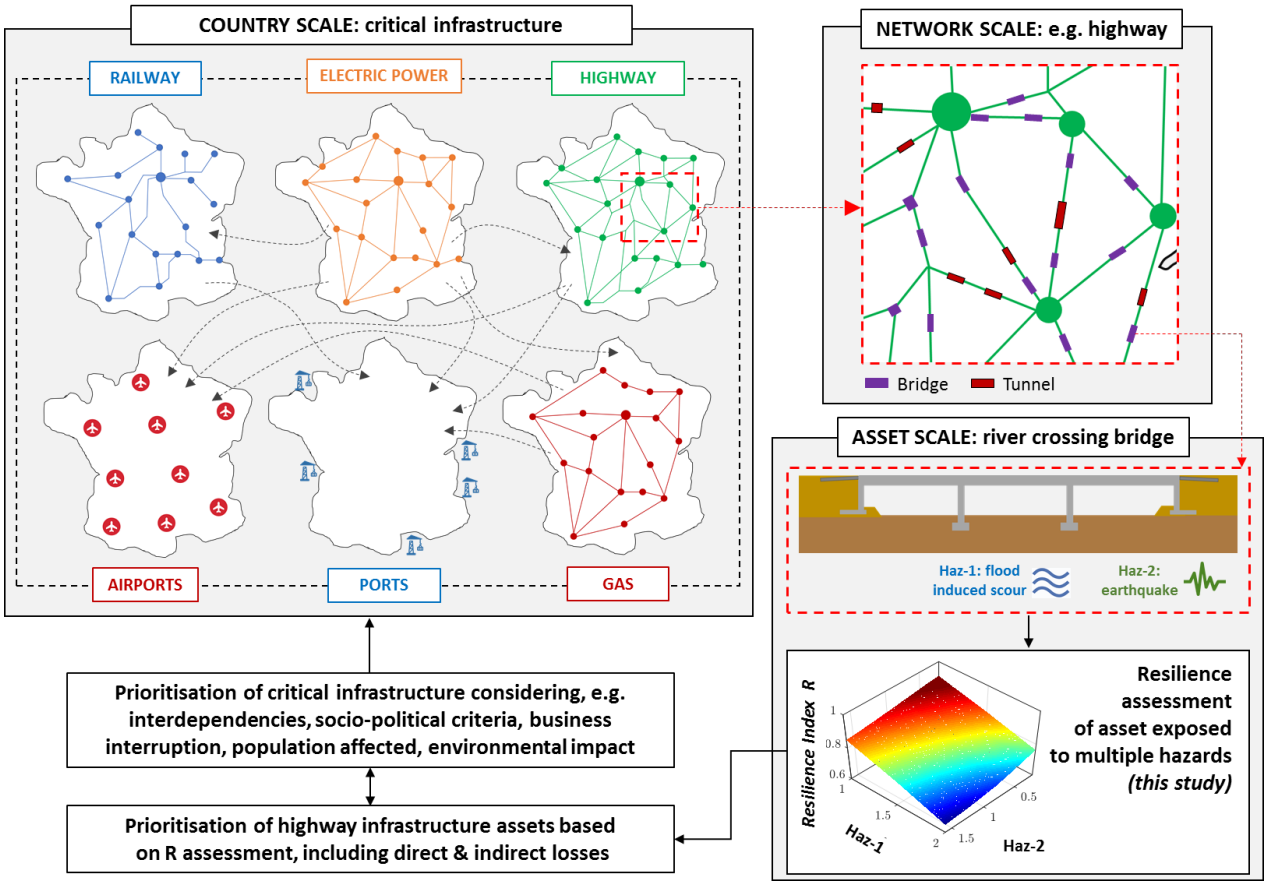

Figure 16. Roadmap of asset-specific resilience-based assessment providing information to network operators and countries for decision-making in resources allocation.

4. Conclusions

This paper proposes an integrated framework for the resilience assessment of infrastructure assets exposed to multiple hazards characterized by diverse nature, impact and occurrence time. The framework accounts for (i) the robustness of the assets to hazard actions, based on realistic fragility functions for individual and multiple hazards, and (ii) the rapidity of the recovery, based on realistic reinstatement and restoration models after

689 individual and multiple hazard events. The framework allows quantifying the impact on the resilience of
690 alternative restoration strategies following the occurrence of a hazardous event, including the cases of full,
691 partial and even no restoration. A generalized index is defined to quantify the resilience in a unified way for
692 different hazard and recovery scenarios. This index can be used to facilitate decision-making and prioritisation
693 processes by infrastructure owners and operators by maximising the resilience of critical infrastructure based
694 on efficient risk mitigation and restoration strategies.

695 The application of the proposed framework is illustrated by considering a realistic case study, consisting of a
696 multi-span highway bridge exposed to two consecutive hazard scenarios, considering flood-induced scour
697 followed by an earthquake. Novel contributions include: 1) the identification of representative failure modes for
698 flood and earthquake hazards, 2) the development of realistic fragility and restoration functions for individual
699 and combined hazards, and 3) the consideration of appropriate restoration tasks. The resilience models are
700 developed for multiple hazard scenarios of different intensities, considering the full or partial recovery of the
701 bridge between the different hazard events and accounting for the uncertainty in the temporal occurrence of the
702 second hazard. Based on the results of the study, the following conclusions are drawn:

703 (1) In all cases studied the mean resilience index decreases by increasing the severity of the two hazards and by
704 reducing the time of occurrence of the second hazard event with respect to the first.

705 (2) The randomness of the temporal occurrence of the second hazard can introduce significant variability in the
706 resilience index, which increases by increasing the severity of both hazards. Based on the application on the
707 bridge, the dispersion of the resilience index was found to be of the order of 8% for relatively low scour hazard
708 occurrences, e.g. a scour depth of 1.0 Df and low earthquake intensities with a PGA of 0.2 g, as the damages
709 induced by the hazards are insignificant. The error in the calculation of the resilience index increases
710 significantly and attained values of 23% for the larger scour depth of 1.5 Df and 33% for the maximum hazard
711 occurrence of 2.0 Df, in conjunction with high earthquake intensities of 1.2 g.

712 (3) Assuming that the asset has fully recovered from the first hazard event when the second hazard event occurs,
713 it results in an overestimation of the resilience index. Thus, multiple hazards occurrences cannot be treated

independently using simple superimposition of resilience indices. Their interaction has to be accounted and the resulting effects have to be considered at each stage of the resilience assessment.

Further research should be carried out to validate the restoration models, based on recorded data, evidence and input from experts, e.g. elicitation approaches, with participation by owners, stakeholders and engineers. Future work will focus on the deployment of this framework for life-cycle resilience assessment of critical infrastructure assets and networks, including utilising monitoring techniques in rapid resilience assessments.

Acknowledgments

This study has received funding by the European Union H2020-Marie Skłodowska-Curie Research Grants Scheme MSCA-IF-2016 (grant agreement No 746298: TRANSRISK-Vulnerability and risk assessment of transportation systems of assets exposed to geo-hazards).

References

Akiyama, M., Frangopol, D. M., Ishibashi, H., 2019. Toward life-cycle reliability-, risk-and resilience-based design and assessment of bridges and bridge networks under independent and interacting hazards: emphasis on earthquake, tsunami and corrosion. Structure and Infrastructure Engineering, https://doi: 10.1080/15732479.2019.1604770.

Almufti I., Willford M.R., 2013. Resilience-Based Earthquake Design (REDi) Rating System. Version 1.0. Arup.

Argyroudis, S., Kaynia, A.M., 2014. Fragility functions of highway and railway infrastructure. In: Pitilakis K, Crowley H, Kaynia AM (eds) SYNER-G: Typology definition and fragility functions for physical elements at seismic risk. GGEE 27, Springer.

Argyroudis, S., Tsinidis, G., Gatti, F., Pitilakis, K., 2017. Effects of SSI and lining corrosion on the seismic vulnerability of shallow circular tunnels. Soil Dynamics Earthquake Engineering 98, 244-256.

Argyroudis, S., Mitoulis, S., Kaynia, A.M., Winter, M.G., 2018. Fragility assessment of transportation infrastructure systems subjected to earthquakes. Geotechnical Special Publication 292, 174-183.

739 Argyroudis, S., Mitoulis, S.A., Winter, M., Kaynia, A.M., 2019. Fragility of transport assets exposed to multiple
740 hazards: State-of-the-art review toward infrastructural resilience. Reliability Engineering and System Safety,
741 191, 106567.

742 Arrighi, C., Pregnolato, M., Dawson, R.J., Castelli, F., 2019. Preparedness against mobility disruption by floods.
743 Science of the Total Environment, 654, 1010-1022.

744 Aygün, B., Duenas-Osorio, L., Padgett, J.E., DesRoches, R., 2011. Efficient longitudinal seismic fragility
745 assessment of a multi-span continuous steel bridge on liquefiable soils. ASCE J. Bridge Eng 16, 93–107.

746 Ayyub, B.M., 2014. Systems resilience for multihazard environments: Definition, metrics, and valuation for
747 decision making. Risk Analysis, 34(2), 340-355.

748 Balomenos, G.P., Padgett, J.E., 2017. Fragility analysis of pile-supported wharves and piers exposed to storm
749 surge and waves. Journal of Waterway, Port, Coastal, and Ocean Engineering, 144(2), 04017046.

750 Banerjee, S., Prasad, G.G., 2013. Seismic risk assessment of reinforced concrete bridges in flood-prone regions.
751 Structure and Infrastructure Engineering, 9, 952-968

752 Billah, A.H.M., Alam, M.S., 2015. Seismic fragility assessment of highway bridges: a state-of-the-art review.
753 Structure and Infrastructure Engineering, 11(6), 804-832.

754 Bocchini, P., Frangopol, D.M., 2012b. Optimal resilience-and cost-based postdisaster intervention prioritization
755 for bridges along a highway segment. Journal of Bridge Engineering, 17(1), 117-129.

756 Bocchini, P., Frangopol, D.M., 2012a. Restoration of bridge networks after an earthquake: multi-criteria
757 intervention optimization. Earthquake Spectra, 28(2), 427-455.

758 Bocchini, P., Frangopol, D.M., Ummenhofer, T., Zinke, T., 2014. Resilience and sustainability of the civil
759 infrastructure: Towards a unified approach. Journal of Infrastructure Systems, 20(2), 04014004, 1-16.

760 Bradley, B.A., M. Cubrinovski, R.P. Dhakal, MacRae, G.A., 2010. Probabilistic seismic performance and loss
761 assessment of a bridge–foundation–soil system. Soil Dynamics and Earthquake Engineering, 30, 395–411.

762 Brandenberg, S.J., Kashighandi, P., Zhang, J., Huo, Y., Zhao M., 2011. Fragility functions for bridges in
763 liquefaction-induced lateral spreads, Earthquake Spectra 27(3), 683–717.

764 Bruneau, M., Barbato, M., Padgett, J., Zaghi, A.E., Mitrani-Reiser, J., Li, Y., 2017. State of the art of
765 multihazard design. Journal of Structural Engineering, 143(10), 03117002.
766 Bruneau, M., Chang, S.E., Eguchi, R.T., Lee, G.C., O'Rourke, T.D., Reinhorn, A.M., Shinozuka, M., Tierney,
767 K., Wallace, W.A., von Winterfeldt, D., 2003. A framework to quantitatively assess and enhance the seismic
768 resilience of communities. Earthquake Spectra, 19(4), 733-752.
769 Castillo, A., 2014. Risk analysis and management in power outage and restoration: A literature survey. Electric
770 power systems research, 107, 9-15.
771 Chan, R., Schofer, J.L., 2015. Measuring transportation system resilience: response of rail transit to weather
772 disruptions. Natural Hazards Review, 17(1).
773 Chang, S., 2016. Socioeconomic impacts of infrastructure disruptions. Oxford Research Encyclopedia of
774 Natural Hazard Science.
775 Chen, G., Huang, K., Zou, M., Yang, Y., Dong, H., 2019. A methodology for quantitative vulnerability
776 assessment of coupled multi-hazard in Chemical Industrial Park. Journal of Loss Prevention in the Process
777 Industries, 58, 30-41.
778 Cimellaro, G.P., Reinhorn, A.M., Bruneau, M., 2010. Framework for analytical quantification of disaster
779 resilience. Engineering Structures, 32(11), 3639-3649.
780 Cimellaro, G.P., Renschler, C., Reinhorn, A.M., Arendt, L. 2016. PEOPLES: a framework for evaluating
781 resilience. Journal of Structural Engineering, 142(10), 04016063.
782 Cimellaro, G.P., Tinebra, A., Renschler, C., Fragiadakis, M., 2015. New resilience index for urban water
783 distribution networks. Journal of Structural Engineering, 142(8), C4015014.
784 Cumbria County Council 2010. Cumbria floods November 2009: an impact assessment.
785 http://www.cumbria.gov.uk/eLibrary/Content/Internet/536/671/4674/4026717419.pdf, last access: October
786 2019.
787 Decò, A., Bocchini, P., Frangopol, D.M. 2013. A probabilistic approach for the prediction of seismic resilience
788 of bridges. Earthquake Engineering & Structural Dynamics, 42(10), 1469-1487.

789 Decò, A., Frangopol, D.M. 2011. Risk assessment of highway bridges under multiple hazards. Journal of Risk
790 Research, 14(9), 1057-1089.

791 Dong, Y, Frangopol, D.M., Saydam, D. 2013. Time-variant sustainability assessment of seismically vulnerable
792 bridges subjected to multiple hazards. Earthquake Engineering and Structural Dynamics, 42:1451–1467.

793 Dong, Y., Frangopol, D.M. 2015. Risk and resilience assessment of bridges under mainshock and aftershocks
794 incorporating uncertainties. Engineering Structures, 83, 198-208.

795 Dong, Y., Frangopol, D.M. 2016. Probabilistic time-dependent multihazard life-cycle assessment and resilience
796 of bridges considering climate change. Journal of Performance of Constructed Facilities, 30(5), 04016034.

797 Draper, S., An, H., Cheng, L., White, D. J., Griffiths, T. 2015. Stability of subsea pipelines during large storms.
798 Philosophical Transactions of the Royal Society A: Mathematical, Physical and Engineering Sciences, 373
799 (2033), 20140106.

800 Elgamal, A., Yan, L., Yang, Z., Conte, J.P. 2008. Three-dimensional seismic response of humboldt bay bridge-
801 foundation-ground system. ASCE Journal of Structural Engineering,134(7), 1165-1176.

802 Faturechi, R., Miller-Hooks, E. 2014. Travel time resilience of roadway networks under disaster. Transportation
803 Research Part B: Methodological, 70, 47–64

804 Faturechi, R., Levenberg, E. and Miller-Hooks, E. 2014. Evaluating and optimizing resilience of airport
805 pavement networks. Computers and Operations Research, 43, 335-348.

806 Fereshtehnejad, E., Shafieezadeh, A. 2016. Multiple hazard incidents lifecycle cost assessment of structural
807 systems considering state-dependent repair times and fragility curves. Earthquake Engineering & Structural
808 Dynamics, 45(14), 2327-2347.

809 Fotopoulou, S.D., Pitilakis, K.D., 2017. Vulnerability assessment of reinforced concrete buildings at precarious
810 slopes subjected to combined ground shaking and earthquake induced landslide. Soil Dynamics &
811 Earthquake Engineering, 93, 84-98.

812 Fotouhi, H., Moryadee, S., Miller-Hooks, E., 2017. Quantifying the resilience of an urban traffic-electric power
813 coupled system. Reliability Engineering and System Safety, 163, 79-94.

814 Franchin, P., 2018. Research Needs Towards a Resilient Community. Theme lecture at the 16th European
815 Conference of Earthquake Engineering, Thessaloniki, Greece, June 18-21.
816 Frangopol, D.M., Bocchini, P., 2011. Resilience as optimization criterion for the bridge rehabilitation of a
817 transportation network subject to earthquake. ASCE Structures Congress 2011, D. Ames, D., T.L. Droessler,
818 M. Hoit, M., eds., ASCE, CD-ROM, 2044-2055.
819 Furlan, E., Torresan, S., Critto, A., Marcomini, A., 2018. Spatially explicit risk approach for multi-hazard
820 assessment and management in marine environment: The case study of the Adriatic Sea. Science of the Total
821 Environment, 618, 1008-1023.
822 Galbusera, L., Giannopoulos, G., Argyroudis, S. and Kakderi, K., 2018. A Boolean Networks approach to
823 modeling and resilience analysis of interdependent critical infrastructures. Computer-Aided Civil and
824 Infrastructure Engineering, 33(12), 1041-1055.
825 Gay, L.F., Sinha, S.K., 2013. Resilience of civil infrastructure systems: literature review for improved asset
826 management. International Journal of Critical Infrastructures, 9(4), 330-350.
827 Ghosh, J., Padgett, J.E, Sánchez-Silva, M., 2015. Seismic damage accumulation of highway bridges in
828 earthquake prone regions, Earthquake Spectra, 31(1), 115-135
829 Giannopoulos, G., Filippini, R., Schimmer, M., 2012. Risk assessment methodologies for critical infrastructure
830 protection. Part I: A state of the art. JRC Technical Notes EUR 25286 EN, Publications Office of the
831 European Union.
832 Gidaris, I., Padgett, J.E., Barbosa, A.R., Chen, S., Cox, D., Webb, B., Cerato, A., 2017. Multiple-hazard fragility
833 and restoration models of highway bridges for regional risk and resilience assessment in the United States:
834 state-of-the-art review. Journal of Structural Engineering, 143(3).
835 Gill, J.C., Malamud, B.D., 2014. Reviewing and visualizing the interactions of natural hazards. Reviews of
836 Geophysics, 52(4), 680-722.
837 Guo, X., Wu, Y., Guo, Y., 2016. Time-dependent seismic fragility analysis of bridge systems under scour hazard
838 and earthquake loads. Engineering Structures, 121,52–60.

839 Hackl, J., Lam, J.C., Heitzler, M., Adey, B.T., Hurni, L., 2018. Estimating network related risks: a methodology
840 and an application in the transport sector. Nat. Hazards Earth Syst. Sci. 18, 2273–2293.
841 HAZUS-MH, 2011. Multi-hazard loss estimation methodology: earthquake model Hazus-MH MR5 technical
842 manual. Federal Emergency Management Agency, Washington, DC.
843 Hosseini, S., Barker, K., Ramirez-Marquez, J.E., 2016. A review of definitions and measures of system
844 resilience. Reliability Engineering & System Safety, 145, 47-61.
845 Huang, H., Zhang, D., 2016. Resilience of operated tunnels under extreme surcharge: field study. Japanese
846 Geotechnical Society Special Publication, 2(42),1492-1496.
847 Hughes, J.F., Healy, K., 2014. Measuring the resilience of transport infrastructure. NZ Transport Agency
848 research report 546, 82pp.
849 Iervolino, I., Massimiliano, G., Barbara, P., 2015. Reliability of structures to earthquake clusters. Bulletin of
850 Earthquake Engineering, 13(4), 983-1002.
851 Iervolino, I., Giorgio, M., Chioccarelli, E., 2016. Markovian modeling of seismic damage accumulation.
852 Earthquake Engineering & Structural Dynamics, 45(3), 441-461.
853 Kameshwar, S., Padgett, J.E., 2014. Multi-hazard risk assessment of highway bridges subjected to earthquake
854 and hurricane hazards. Engineering Structures, 78, 154-166.
855 Kameshwar, S., Padgett, J.E., 2018. Response and fragility assessment of bridge columns subjected to barge-
856 bridge collision and scour. Engineering Structures, 168, 308-319.
857 Karamlou A., Bocchini, P., 2017. Functionality-Fragility Surfaces. Earthquake Engineering and Structural
858 Dynamics, 46(10).
859 Karamlou, A., Ma, L., Sun, W., Bocchini, P., 2017. Generalized probabilistic restoration prediction. In: C
860 Bucher, BR Ellingwood, DM Frangopol (Editors), Proc of the 12th Int. Conf. on Structural Safety and
861 Reliability, Vienna, Austria, 6–10 August, ISBN 978-3-903024-28-1.
862 Kayen, R., Brandenberg, S.J., Collins, B.D., Dickenson, S., Ashford, S., Kawamata, Y., Tanaka, Y., Koumoto,
863 H., Abrahamson, N., Cluff, L. and Tokimatsu, K., 2009. Geoengineering and seismological aspects of the
864 Niigata-Ken Chuetsu-Oki earthquake of 16 July 2007. Earthquake Spectra, 25(4), 777-802.

865 Kiel J. et al., 2016. A decision support system for the resilience of critical transport infrastructure to extreme
866 weather events. Transportation Research Procedia, 14, 68-77.

867 Kirby, A.M., Roca, M., Kitchen, A., Escarameia, M., Chesterton, O.J., 2015. Manual on scour at bridges and
868 other hydraulic structures, 2nd edn., CIRIA Report C742, CIRIA, London.

869 Komendantova, N., Mrzyglocki, R., Mignan, A., Khazai, B., Wenzel, F., Patt, A., Fleming, K., 2014. Multi-
870 hazard and multi-risk decision-support tools as a part of participatory risk governance: Feedback from civil
871 protection stakeholders. International Journal of disaster risk reduction, 8, 50-67.

872 Kong, J., Simonovic, S.P., 2019. Probabilistic multiple hazard resilience model of an interdependent
873 infrastructure system. Risk Analysis, https://doi.org/10.1111/risa.13305

874 Krausmann, E., Cruz A.M., 2013. Impact of the 11 March 2011, Great East Japan earthquake and tsunami on
875 the chemical industry. Natural Hazards, 67(2), 811-828.

876 Kumar, R., Gardoni, P. 2011. Modeling structural degradation of RC bridge columns subjected to earthquakes
877 and their fragility estimates. Journal of Structural Engineering, 138(1), 42-51.

878 Lam, J.C., Adey, B.T., Heitzler, M., Hackl, J., Gehl, P., van Erp, N., D'Ayala, D., van Gelder, P., Hurni, L.,
879 2018. Stress tests for a road network using fragility functions and functional capacity loss functions.
880 Reliability Engineering and System Safety, 173, 78-93.

881 Li, Y., Song, R., van De Lindt, J.W., 2014. Collapse fragility of steel structures subjected to earthquake
882 mainshock-aftershock sequences. Journal of Structural Engineering, 140(12), p.04014095.

883 Linkov, I., Bridges, T., Creutzig, F., Decker, J., Fox-Lent, C., Kröger W., et al., 2014. Changing the resilience
884 paradigm. Nature Climate Change, 4(6), 407.

885 Liu, B., Siu, Y.L., Mitchell, G., 2016. Hazard interaction analysis for multi-hazard risk assessment: a systematic
886 classification based on hazard-forming environment. Natural Hazards and Earth System Sciences, 16(2),
887 629-642.

888 Lloyd's Register Foundation 2015. Foresight review of resilience engineering, Report Series: No. 2015.2.

889 Luna, R., Balakrishnan, N., Dagli, C.H. 2011. Postearthquake recovery of a water distribution system: discrete
890 event simulation using colored petri nets. Journal of Infrastructure Systems, 17(1), 25-34.

891 Martin, J., Alipour, A., Sarkar, P., 2019. Fragility surfaces for multi-hazard analysis of suspension bridges under
892 earthquakes and microbursts. Engineering Structures, 197, 109169.
893 Marzocchi, W., Garcia-Aristizabal, A., Gasparini, P., Mastellone, M., Di Ruocco, A., 2012. Basic principles of
894 multi-risk assessment: a case study in Italy. Nat Hazards, 1-23.
895 Matlab (2017). Matlab R2017a, The MathWorks, Inc., Natick, Massachusetts, United States.
896 Matthews, E.C., Sattler, M., Friedland, C.J., 2014. A critical analysis of hazard resilience measures within
897 sustainability assessment frameworks. Environmental Impact Assessment Review, 49, 59-69.
898 Mebarki, A., Jerez, S., Prodhomme, G., Reimeringer, M., 2016. Natural hazards, vulnerability and structural
899 resilience: tsunamis and industrial tanks. Geomatics, Natural Hazards and Risk, 7(sup1), 5-17.
900 Mensah, A.F., Dueñas-Osorio, L., 2015. Efficient resilience assessment framework for electric power systems
901 affected by hurricane events. Journal of Structural Engineering 142(8), C4015013.
902 Ming, X., Xu,W., Li, Y., Du, J., Liu, B., Shi, P., 2015. Quantitative multi-hazard risk assessment with
903 vulnerability surface and hazard joint return period. Stochastic, Environmental Research & Risk Assessment,
904 29(1), 35–44.
905 Mitoulis, S., Argyroudis, S., Lamb, R., 2019. Risk and resilience of bridgeworks exposed to hydraulic hazards,
906 Proc. of IABSE2019-New York, September 4-6.
907 Moghadas, M., Asadzadeh, A., Vafeidis, A., Fekete, A. and Kötter, T., 2019. A multi-criteria approach for
908 assessing urban flood resilience in Tehran, Iran. International Journal of Disaster Risk Reduction, p.101069.
909 Murphy, B., Yarnold, M., 2018. Temperature-Driven Structural Identification of a Steel Girder Bridge With an
910 Integral Abutment. Engineering Structures, 155, 209-221.
911 NIST, 2016. Community resilience planning guide for buildings and infrastructure systems. NIST Special
912 Publication 1190, National Institute of Standards and Technology,
913 http://dx.doi.org/10.6028/NIST.SP.1190v1
914 Omidvar, B., Kivi, H.K. 2016. Multi-hazard failure probability analysis of gas pipelines for earthquake shaking,
915 ground failure and fire following earthquake. Natural Hazards, 82(1), 703–720.

916 Ouyang, M., Dueñas-Osorio, L., Min, X., 2012. A three-stage resilience analysis framework for urban
917 infrastructure systems. Structural Safety, 36, 23-31.
918 Ouyang, M., Wang, Z., 2015. Resilience assessment of interdependent infrastructure systems: With a focus on
919 joint restoration modeling and analysis. Reliability Engineering and System Safety, 141, 74-82.
920 Padgett J.E., DesRoches R., 2007. Bridge functionality relationships for improved seismic risk assessment of
921 transportation networks. Earthquake Spectra 23(1), 115–130.
922 Padgett, J.E., DesRoches, R. 2009. Retrofitted bridge fragility analysis for typical classes of multispan bridges.
923 Earthquake Spectra, 25(1), 117–141.
924 Padgett, J.E., DesRoches, R., Nielson, B., Yashinsky, M., Kwon, O.-S., Burdette, N., Tavera, E. 2008. Bridge
925 damage and repair costs from hurricane Katrina. Journal of Bridge Engineering, 13(1), 6-14.
926 Pant, R., Thacker, S., Hall, J.W., Alderson, D., Barr, S., 2018. Critical infrastructure impact assessment due to
927 flood exposure. Journal of Flood Risk Management, 11, 22-33.
928 Panteli, M., Pickering, C., Wilkinson, S., Dawson, R., Mancarella, P., 2017. Power system resilience to extreme
929 weather: fragility modeling, probabilistic impact assessment, and adaptation measures. IEEE Transactions
930 on Power Systems, 32(5), 3747-3757.
931 Pescaroli, G., Alexander, D., 2016. Critical infrastructure, panarchies and the vulnerability paths of cascading
932 disasters. Natural Hazards, 82(1), 175-192.
933 Pitilakis, K., Crowley, H., Kaynia, A.M. (eds), 2014. SYNER-G: typology definition and fragility functions for
934 physical elements at seismic risk. Geotechnical, Geological and Earthquake Engineering 27, Springer.
935 Pregnolato, M., Sarhosis, V., Kilsby, C., 2018, Transport resilience to flood-induced bridge failures. EPiC Series
936 in Engineering, 3, 1698-1702.
937 Rockefeller Foundation, 2019. “100 resilient cities”. http://www.100resilientcities.org, accessed: October 2019
938 Scozzese, F., Ragni, L., Tubaldi, E, Gara, F., 2019. Modal properties variation and collapse assessment of
939 masonry arch bridges under scour action. Engineering Structures, 10.1016/j.engstruct.2019.109665

940 Robinne, F.N., Bladon, K.D., Miller, C., Parisien, M.A., Mathieu, J. and Flannigan, M.D., 2018. A spatial
941 evaluation of global wildfire-water risks to human and natural systems. Science of the Total Environment,
942 610, 1193-1206.

943 Rockefeller Foundation, ARUP, 2014. City Resilience Framework.
944 http://publications.Arup.com/Publications/C/City_Resilience_Framework.asp

945 Rus, K., Kilar, V., Koren, D., 2018. Resilience assessment of complex urban systems to natural disasters: a new
946 literature review. Int. J. Disaster Risk Reduct. 31.

947 Sajjad, M., Chan, J.C., 2019. Risk assessment for the sustainability of coastal communities: A preliminary study.
948 Science of the Total Environment, 671, 339-350.

949 Salman, A.M, Li, Y., 2018. A probabilistic framework for multi-hazard risk mitigation for electric power
950 transmission systems subjected to seismic and hurricane hazards, Structure and Infrastructure Engineering,
951 14(11), 1499-1519.

952 Sarkodie, S.A., Strezov, V., 2019. Economic, social and governance adaptation readiness for mitigation of
953 climate change vulnerability: Evidence from 192 countries. Science of the Total Environment, 656, 150-164.

954 Saydam, D., Bocchini, P., Frangopol, D.M. 2013. Time-dependent risk associated with highway bridge
955 networks. Engineering Structures, 54, 221-233.

956 Silva, V., Akkar, S., Baker, J., Bazzurro, P., Castro, J.M., Crowley, H., Dolsek, M., Galasso, C., Lagomarsino,
957 S., Monteiro, R., Perrone, D., 2019. Current Challenges and Future Trends in Analytical Fragility and
958 Vulnerability Modelling. Earthquake Spectra. https://doi.org/10.1193/042418EQS101O

959 Stefanidou S., Kappos A.J., 2019. Bridge-specific fragility analysis: when is it really necessary? Bulletin of
960 Earthquake Engineering,17(4), 2245-2280.

961 Stefanidou, S.P., Kappos, A.J., 2017. Methodology for the development of bridge- specific fragility curves.
962 Earthquake Engineering and Structural Dynamics, 46(1), 73-93.

963 Stern, P.C., Ebi, K.L., Leichenko, R., Olson, R.S., Steinbruner, J.D., Lempert, R., 2013. Managing risk with
964 climate vulnerability science. Nature Climate Change, 3(7), 607.

965 Suzuki, A., Iervolino, I., Kurata, M., Shimmoto, S., 2017. State-dependent fragility curves for aftershock
966 seismic risk assessment of Japanese steel frames. 16WCEE 2017, Santiago Chile, January 9-13, Paper
967 N°1307.

968 Takahashi, Y., Kiureghian, A.D., Ang, A.H.S., 2004. Life-cycle cost analysis based on a renewal model of
969 earthquake occurrences. Earthquake Engineering & Structural Dynamics, 33(7), 859-880.

970 Tang, C., Zhu, J., Qi, X., 2011. Landslide hazard assessment of the 2008 Wenchuan earthquake. Canadian
971 Geotechnical Journal 48, 128-145.

972 Theocharidou, M., Giannopoulos, G., 2015. Risk assessment methodologies for critical infrastructure
973 protection. Part II: A new approach. Tech. Report EUR 27332 EN, Publications Office of the European
974 Union, doi:10.2788/621843.

975 Tubaldi, E., Macorini, L., Izzuddin, B.A., 2018. Three-dimensional mesoscale modelling of multi-span masonry
976 arch bridges subjected to scour. Engineering Structures 165, 486-500.

977 Lloyd's Register Foundation, 2019. The Resilience Shift. https://www.resilienceshift.org/, assecced: October
978 2019.

979 Tsionis, G., Fardis, M.N. 2014. Fragility functions of road and railway bridges. In: Pitilakis K, Crowley H,
980 Kaynia AM (eds) SYNER-G: Typology definition and fragility functions for physical elements at seismic
981 risk. Geotechnical, Geological and Earthquake Engineering 27, Springer Netherlands.

982 Tubaldi, E., Macorini, L., Izzuddin, B. A., Manes, C., Laio, F. 2017. A framework for probabilistic assessment
983 of clear-water scour around bridge piers. Structural Safety, 69, 11-22.

984 UNISDR, 2015. Sendai framework for disaster risk reduction 2015–2030.
985 https://www.unisdr.org/files/43291_sendaiframeworkfordrren.pdf

986 Wang Z., Dueñas-Osorio L., Padgett J.E, 2014. Influence of scour effects on the seismic response of reinforced
987 concrete bridges. Engineering Structures 76, 202–14.

988 Wang, J., Zuo, W., Rhode-Barbarigos, L., Lu, X., Wang, J., Lin, Y., 2019. Literature review on modeling and
989 simulation of energy infrastructures from a resilience perspective. Reliability Engineering and System Safety
990 183, 360-373.

991 Wilson, G., Wilson, T.M., Deligne, N.I., Blake, D.M., Cole, J.W., 2017. Framework for developing volcanic
992 fragility and vulnerability functions for critical infrastructure. Journal of Applied Volcanology, 6(1).
993 Winter M.G., Shearer, B., Palmer, D., Peeling, D., Harmer, C., Sharpe, J., 2016. The Economic Impact of
994 Landslides and Floods on the Road Network. Procedia Engineering, 143, 1425-34.
995 Woods, D.D., 2015. Four concepts for resilience and the implications for the future of resilience engineering.
996 Reliability Engineering and System Safety, 141, 5-9.
997 Yang, D.Y., Frangopol, D.M., 2018. Bridging the gap between sustainability and resilience of civil
998 infrastructure using lifetime resilience, Chapter 23 in Routledge Handbook of Sustainable and Resilient
999 Infrastructure, P. Gardoni, ed., Routledge, 419-442.
000 Yang, D. Y., Frangopol, D.M., 2019a. Societal risk assessment of transportation networks under uncertainties
001 due to climate change and population growth. Structural Safety, 78, 33-47.
002 Yang, D.Y., Frangopol, D.M., 2019b. Risk-based portfolio management of civil infrastructure assets under deep
003 uncertainties associated with climate change: A robust optimization approach, Structure and Infrastructure
004 Engineering, doi: 10.1080/15732479.2019.1639776.
005 Yeo, G.L., Cornell, C.A., 2009. Building life-cycle cost analysis due to mainshock and aftershock occurrences.
006 Structural Safety 31, 396–408.
007 Yilmaz, T., Banerjee, S., Johnson, P.A., 2016. Performance of two real-life California bridges under regional
008 natural hazards. Journal of Bridge Engineering 21(3).
009 Zaghi, A.E., Padgett, J.E., Bruneau, M., Barbato, M., Li, Y., Mitrani-Reiser, J., McBride, A., 2016. Establishing
010 common nomenclature, characterizing the problem, and identifying future opportunities in multihazard
011 design. J. Struct. Eng., 142(12), H2516001.
012 Zanini, M.A., Faleschini, F., Zampieri, P., Pellegrino, C., Gecchele, G., Gastaldi, M., Rossi, R., 2017. Post-
013 quake urban road network functionality assessment for seismic emergency management in historical centres.
014 Structure and Infrastructure Engineering 13(9), 1117-1129.
015 Zhang, S., Wang, G., Sa, W., 2013. Damage evaluation of concrete gravity dams under mainshock–aftershock
016 seismic sequences. Soil Dynamics and Earthquake Engineering, 50, 16-27.

017 Zhang, X., Song, J., Peng, J., Wu, J., 2019. Landslides-oriented urban disaster resilience assessment—A case
018 study in ShenZhen, China. Science of the Total Environment, 661, 95-106.
019 Zhong, J., Gardoni, P., Rosowsky, D., 2012. Seismic fragility estimates for corroding reinforced concrete
020 bridges. Structure and Infrastructure Engineering 8(1), 55-69.
021 Zhu, B., Frangopol, D.M., 2012. Reliability, redundancy and risk as performance indicators of structural
022 systems during their life-cycle. Engineering Structures, 41, 34-49.